Data-driven two-stage robust optimization dispatching model and benefit allocation strategy for a novel virtual power plant considering carbon-green certificate equivalence conversion mechanism

Liwei Ju[a, b*], ShuoShuo Lv[a, b], Xin Qi[a,b], Gen Li [c], Wei Gan[d], Xinlei Zhang[a, b]

a. School of Economics and Management, North China Electric Power University, Changping Beijing, 102206, China

b. Beijing Key Laboratory of New Energy and Low-Carbon Development (North China Electric Power University), Changping Beijing, 102206, China

c. Department of Engineering Technology and Didactics, Technical University of Denmark (DTU), 2750 Ballerup, Denmark

d. School of Engineering, Cardiff University, Cardiff, CF24 3AA, United Kingdom

*Correspondence: jlw@ncepu.edu.cn. Tel.: +86-176-0016-0816

Abstract: With the large-scale integration of distributed energy resources into the distribution network, virtual power plant clusters (VPPs) control based on "intra-group autonomy and inter-group coordination" can reduce the difficulty of grid operation and control. Effective cluster partitioning is the key to realize the optimal operation of VPPs. Based on different types of distributed energy flexibility output models, this paper firstly proposes the aggregation optimization strategy for VPPs. Additionally, A two-stage robust scheduling optimization model for VPPs is proposed. This model accounts for the uncertainties associated with new energy power generation and leverages complementarities in VPPs. The solution algorithm is constructed through the integration of strong dyadic theory and the C&CG algorithm. Then, an equilibrium distribution strategy for the synergistic benefits of VPPs is proposed. Finally, an example analysis is carried out in Huangyuan County, Xining City, Qinghai Province, China. The results show that: (1) The proposed structure-function aggregation optimization strategy enhances the active power balance rate of the VPPs by 23.52%, reduces the aggregate upward flexibility deficit by 56.49% and the aggregate downward flexibility deficit by 76.47%. (2) The proposed two-stage scheduling optimization model for VPPs reduces the required balancing power by 58.37%. At the same time, it decreases the total cost of VPPs by 21.42%, and lowers the average cost of supplying energy to 58.68¥/MW. (3) Utilizing the proposed synergistic benefit allocation strategy, the profits obtained by VPPs for 45.49%, 26.03%, and 28.49% of the total incremental gains. Non-Adjustable Generation Unit (Non-AGU) needs to make a profit of 29.09¥/MWh due to the uncertainty of output. Adjustable Generation Unit (AGU), Energy Storage Device (ESD) and Adjustable Load (AL) gain 6.24¥/MWh, 18.16¥/MWh, and 4.67¥/MWh. Overall, the two-stage scheduling optimization model and benefit allocation strategy for VPPs aggregated by multidimensional information indicators can promote the aggregation of distributed energy resources. It is conducive to the overall energy structure transformation.

Key words: virtual power plant clusters; cluster aggregation optimization; two-stage robust optimization; two-layer benefit allocation.

1 Introduction

Under the background of the dual-carbon target and new power system construction, massive, heterogeneous, dispersed and ubiquitous distributed resources continue to emerge[1]. However, aggregating and coordinating these resources effectively is challenging, which hampers the formation of a stable source-load balance and limits their contribution to the emerging power system[2]. Virtual Power Plant (VPP), serving as integrators of distributed energy, provide a new way of thinking to realize a large number of distributed energy sources to be connected to the grid[Error! Reference source not found.]. VPPs usually existing in clusters in the distribution system. Consequently, designing VPPs tailored to the actual distribution network with specific

flexibility capacities significant importance in advancing the construction of new power systems[Error! Reference source not found.].

In recent years, VPPs mainly take advantage of the decentralized autonomy and regional collaboration capabilities of swarm intelligence. This abilities helps them address the challenges of task scheduling, resource allocation, and behavior coordination among large-scale distributed resources in complex dynamic environments. At present, both domestic and international scholars have conducted extensive research on VPPs. The results primarily focus on three aspects: dynamic aggregation, operation optimization and benefit distribution. In terms of dynamic aggregation, the key lies in determining indicators based on cluster boundary division to facilitate the realization of VPP dynamic aggregation. Presently, cluster boundary division predominantly considers the degree of electrical coupling between nodes[5]. Fu X et al.[6] constructed a reactive voltage partition model based on the node conductance matrix of the grid, and use k-means algorithms to obtain the results of cluster partitioning. Zheng F et al.[7] established a weighted network model based on electrical distance. It incorporates incorporating both topological and electrical characteristics, and using the modularity as the objective function for reactive power partitioning. However, the results of clustering based on electrical distance are highly dependent on the network structure, necessitating a more comprehensive clustering scheme based on the clustering index system. Marcos T et al.[8] proposed a novel cluster classification system considering the electrical coupling and power matching characteristics. This system incorporates module degree scale and reactive power and active power balance indicators for classification from structural and functional perspectives. Ruth D et al.[Error! Reference source not found.] introduced an modularity indicator considering local reactive power balance capability for distribution network cluster division, addressing overvoltage issues by controlling cluster voltages. Hu D et al.[10] proposed reactive power reserve index and modularity index to establish reactive power partitioning based on day-ahead scheduling. Most of the literature focused on cluster division to address voltage control and achieves commendable results[11]. However, the high proportion of distributed energy access also affects the optimal operation of the distribution network[12]. The existing clustering approaches do not consider the level of active power coordination in the distribution network or the flexibility and complementary characteristics among different nodes. Therefore, this paper proposes to consider the structure-function aggregation optimization strategy for VPPs to improve the flexibility and complementary capability of the cluster division scheme.

In terms of operational optimization, existing studies have mainly focused on minimizing costs[Error! Reference source not found.] maximizing benefit[Error! Reference source not found.] or environmental sustainability[14]. For example, Ramea K et al.[Error! Reference source not found.] constructed a scheduling optimization model for VPP in networks with plug-in hybrid electric vehicles, aiming to minimize costs and carbon dioxide emissions. Furthermore, the predictability of uncertain random variables has the property of gradually increasing as the time domain approaches[17]. Recent studies have explored different time scales such as day-ahead and Real-time, constructing robust scheduling optimization models for VPPs. For example, Ding B et al.[Error! Reference source not found.] proposed a multi-time scale robust optimal scheduling method. It achieves the goal of minimizing total cost and maximizing data uncertainty tolerance under ellipsoidal uncertainty sets. Ma C et al.[19]designed a multi-time scale operational scheduling optimization model for VPPs, incorporating profit in the day-ahead market and expectations of reward and punishment in the intra-day market. However, conventional multi-timescale optimal scheduling models often overlook system robustness. Existing robust optimization models tend to focus solely on extreme worst-case scenarios, resulting in conservative scheduling schemes that may compromise the economic efficiency of VPP[20]. To address this, the two-stage robust optimization model emerges as a flexible solution capable of striking a balance between economy and robustness[Error! Reference source not found.]. For example, Zhang Y et al.[22]applied a two-stage robustness approach to optimize the scheduling of VPP participating in the electricity market. It demonstrates the advantage of the two-stage robustness in mitigating conservatism in the system's optimal scheduling outcomes. Additionally, the research objects of the above research subjects focused on single VPP and did not account for the mutual aid capability of VPPs

within actual distribution networks. Therefore, this paper proposes the construction of a two-stage scheduling optimization model tailored for VPPs to address this gap in the literature.

In terms of benefit allocation, the optimal operation of VPPs relies on the co-operation of multiple actors. How to establish a scientific and reasonable benefit allocation method is the key to guarantee the sustainable operation of VPPs. The Shapley value method is a commonly used method to solve the benefit allocation problem based on the co-operative game[Error! Reference source not found.]. Pu et al.[24] reviewed the origin and evolution of Shapley's value, summarizing its current applications across various domains. Zhou D[25] , Zhao L[26] and Diva A[27] employed the Shapley value method to allocate incremental benefits in wind-power-storage-heat systems, combined heat and power systems, and energy bases. Chen Y et al. [28] redistributed benefits from local energy transactions using the Shapley value method in conjunction with bargaining methods. Ju L et al. [29] utilized an improved Shapley value method to allocate power sales revenue. However, the Shapley value method primarily assesses the contribution of different participants to cooperative costs or benefits, overlooking risk or environmental contribution. To address this limitation, scholars have proposed modifications, such as incorporating risk factors or cost factors into the Shapley value method for energy unit cooperation benefit allocation. Yang S et al[30] incorporated the risk factor into the Shapley value method for the benefit allocation of different energy units' co-operation. Pan H[31] proposed the cost factor and use it for multi-energy service provider cooperative benefit allocation. Diego G et al[Error! Reference source not found.] introduced improvement factors such as contribution to net load and net output size, and proposed a method of determining the weights of the improvement factors based on the entropy value method. This method achieves the improvement of the traditional Shapley value method. Nevertheless, the traditional benefit allocation strategy fails to consider multi-level subject benefit allocation, limiting its direct applicability to the benefit allocation problems of VPPs. Therefore, this paper proposes an improved two-layer benefit allocation method to address the challenge of achieving balanced benefit allocation within VPPs.

Based on the above analysis, Scholars both domestically and internationally have conducted extensive research on the optimal operation of VPPs. Their findings are pertinent for decision-making in dynamic aggregation, operational optimization, and benefit distribution. However, existing research exhibits certain gaps. Firstly, most of literatures rely solely on electrical distance between nodes as the criterion for VPP aggregation. This approach overlooks the coordinated and complementary attributes of distributed energy resources, leading to VPP clusters lacking in flexibility and economic viability. Secondly, in terms of operation optimization, while robust stochastic optimization methods have been increasing, these studies often fail to bridge scheduling correlation between the day-ahead and real-time stages. Moreover, they neglect to consider the interconnection capacity of VPP clusters within the actual distribution network. Addressing this requires extending single-stage robust scheduling optimization models for VPPs and integrating VPP cluster interconnection capability into two-stage robust scheduling optimization models. Finally, the existing literatures do not consider the benefit allocation problem of multi-level subjects. To fill these gaps, this paper proposes a two-stage scheduling optimization model and benefit allocation strategy for virtual power plant clusters aggregated by multidimensional information indicators. The key contributions of this paper are outlined below:

(1) Proposed a structural-functional aggregation optimization strategy for VPPs. Structural indicators, including modularity metrics based on electrical distances, and functional indicators including power balance degree, flexibility supply and demand balance indicator, and probabilistic flexibility risk indicator, guide the division of VPPs. They provide a rational basis for VPPs division.

(2) Proposed a two-stage robust optimization model for VPPs and strong duality theorem, C&CG solution algorithm. The robust coefficients are used to construct the uncertainty set for new energy output. Then, a two-stage robust scheduling optimization model of VPPs is constructed with the objective function of minimizing the average energy generation cost. Finally, the two-layer optimization model is transformed into a single-layer model using the strong dyadic theory, and the C&CG algorithm is used to solve the optimization model.

(3) Proposed a balanced allocation strategy for two-stage benefits of VPPs. Using the Shapley value method, the incremental benefits of the external cooperation subjects of VPPs are taken as characteristic values for the weights of the benefits allocation. Additionally, risk and cost factors are introduced to enhance the Shapley method. An improved two-layer benefits allocation method is proposed to solve the challenge of balanced benefits allocation within VPPs.

The remainder of the paper is organized as follows: Section 2 describes VPPs structure and mathematically models. Section 3 proposes structure-function aggregation strategy for VPPs. Section 4 constructs a two-stage scheduling optimization model for VPPs. Section 5 proposes the VPPs synergistic benefit allocation strategy considering the multi-level subject cooperation game. Section 6 selects an actual distribution network in the Huangyuan county as a simulation system to verify the effectiveness and applicability of the constructed model. Section 7 highlights the contributions and conclusions of the paper.

2 VPPs structure and unit model

2.1 VPPs structure

VPPs integrates the characteristics of distributed energy sources in the distribution network. Each VPP can operate with internal consistency and also cooperate with external clusters. This setup offers a more effective solution to the challenges of integrating distributed energy into the grid, as well as the communication and computational issues associated with centralized control. Therefore coordinated operation within VPPs is particularly important in grid operation. Fig. 1 illustrates the VPPs structure within the distribution network.

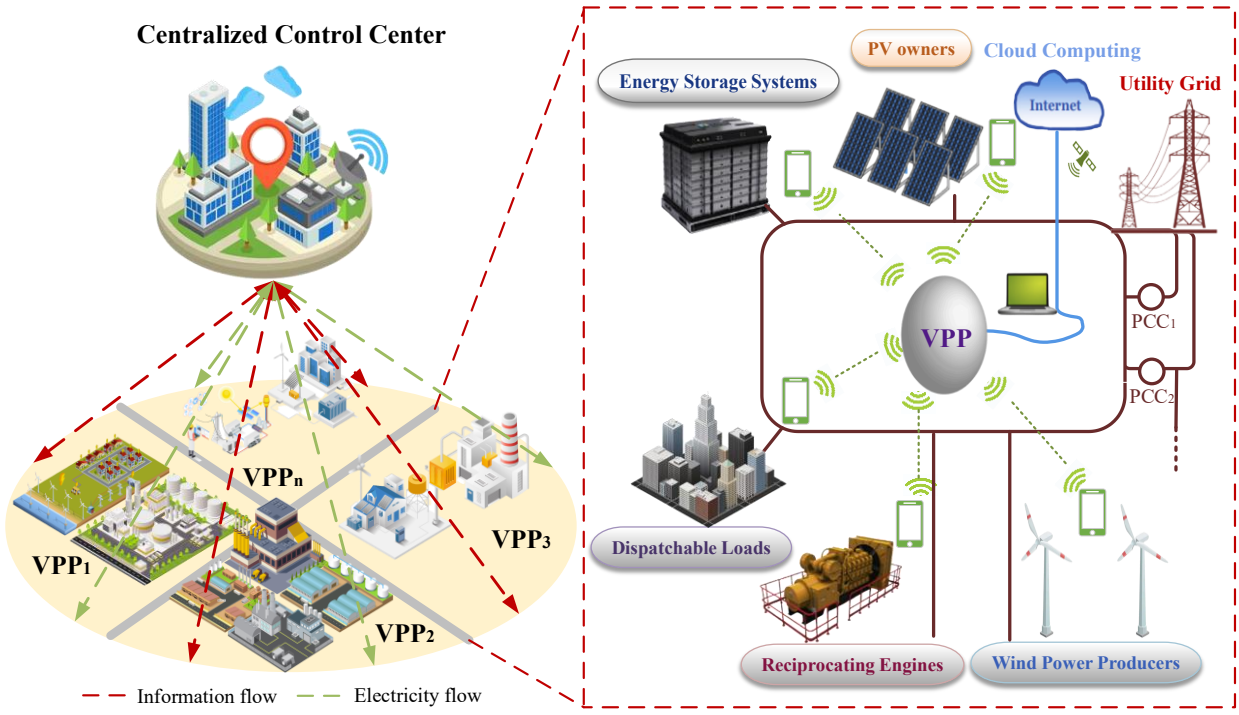

Fig.1 VPPs structure

2.2 VPPs model

VPPs is proposed to integrate various distributed energy sources, including DR, ESD and AL. Among them, distributed power sources include adjustable and Non-adjustable generation units.

(1) Non-AGU

Non-AGU are mainly stochastic distributed power sources represented by WPP and PV. Its output largely relies on external natural conditions, such as wind speed and solar radiation intensity. In this paper, wind power and photovoltaic power generation‘s specific models are as follows:

$$P_{WPP,t}=\begin{cases}0 & ,v_t<v_{\text{cut-in}}\ \&\ v_t\geq v_{\text{cut-out}}\\ \dfrac{v_t^3-v_{\text{cut-in}}^3}{v_R^3-v_{\text{cut-in}}^3}P_{WPP,\text{R}} & ,v_{\text{cut-in}}<v_t<v_{\text{R}}\\ P_{WPP,\text{R}} & ,v_R<v_t<v_{\text{cut-out}}\end{cases} \tag{1}$$

Where: $P_{WPP,t}$ is the generation output of WPP at time *t*; v_t is the natural wind speed at time *t*; v_{in} and v_{out} are the cut-in and cut-out wind speeds; v_{rated} is the rated wind speed; $P_{WPP,\text{R}}$ is the rated wind speed of WPP.

$$P_{PV,t}=\left[1\text{-}\gamma_T\left(T_{\text{air}}+\frac{T_{\text{n}}\text{-}20}{800}R_t-T_{\text{ref}}\right)\right]\eta_{\text{ref}}N_{PV}A_{PV}R_t \tag{2}$$

Where: $P_{PV,t}$ is the PV generation output at time *t*; γ_T is the temperature parameter of PV panel conversion efficiency; T_{air} is the ambient temperature; T_{n} is the normal operating temperature; R_t is the solar radiation intensity at time *t*; T_{ref} is the reference temperature; η_{ref} is the reference efficiency; N_{PV} is the number of PV panels; A_{PV} is the area of the PV panel.

(2) AGU

AGU are mainly controllable units represented by gas turbines, diesel power generation. If the small hydropower station is equipped with storage tanks, it also has the regulating performance, similar to the mode of operation of the energy storage. This paper specifically examines gas turbines and diesel generators as adjustable power supplies. The power generation output is influenced by factors such as fuel consumption and power generation pressure. The specific model is as follows:

$$P_{AGU,t}=\partial_0+\partial_1F_{\text{p}}+\partial_2F_{AGU,t}+\partial_3F_{\text{p}}^2 \tag{3}$$

Where: $P_{AGU,t}$ is the output power of AGU at time *t*; F_{p} is the pressure of biogas generation. $F_{AGU,t}$ is the fuel consumption of AGU at time *t*; ∂_0 is the constant term coefficient; ∂_1 and ∂_2 are the linear term coefficients of the pressure and fuel consumption; ∂_3 is the quadratic term coefficient.

(3) ESD

ESD is configured with a battery to perform charging during the load valley hours and discharging during the load peak hours, thus responding to the optimal scheduling of the VPP. The specific model is as follows:

$$P_{ESD,t}=\left(1\text{-}\eta_{ESD}^{+}\right)P_{ESD,t}^{+}\text{-}P_{ESD,t}^{-}\Big/\left(1\text{-}\eta_{ESD}^{-}\right) \tag{4}$$

Where: $P_{ESD,t}$ is the output power of ESD at time *t*; η_{ESD}^{-} and η_{ESD}^{+} are ESD charging/discharging loss rate; $P_{ESD,t}^{-}$ and $P_{ESD,t}^{+}$ are ESD charging/discharging power at time *t*.

(4) AL

AL participate in VPP dispatch optimization mainly through price-based demand response and incentive-based demand response, which are expressed in the form of interruptible and incentive loads. The specific model is as follows:

$$P_{AL,t}=-\eta_{\text{off}}P_{AL,t}^{-}+\eta_{\text{on}}P_{AL,t}^{+} \tag{5}$$

Where: $P_{AL,t}$ is the dispatch power of the adjustable load at time *t*; $P_{AL,t}^{-}$ and $P_{AL,t}^{+}$ are the dispatch power of the adjustable load to provide interruptible and excitable loads; η_{on} and η_{off} are the excitable and interruptible states of the adjustable load.

3 Optimization strategy for Structural-Functional aggregation in VPPs

3.1 S cluster aggregation indicators

VPP contains Non-AGU, AGU, ESD and AL. How to balance the structure and risk of cluster aggregation is the key to the cluster division. Consequently, this paper opts for the structure and functionality as the cluster aggregation indicators.

3.1.1 Structural indicators

This paper employs the electrical distance-based modularity indicator to characterize the structural aspects of VPPs aggregation. The modularity indicator quantifies the probability of two network nodes falling within the same region, as follows:

$$\varphi_{\text{str}}=\frac{1}{2M}\sum_{i\in N}\sum_{j\in N}\left(d_{ij}-\frac{m_i m_j}{2M}\right)\delta(i,j) \tag{6}$$

Where: φ_{str} is the modularity indicator; m_i and m_j are the sum of edge rights connected with node *i* and node *j*; $\delta(i,j)$ is the regional relationship between node *i* and node *j*. When node *i* and node *j* are in the same region, $\delta(i,j)$ =1, vice versa $\delta(i,j)$ =0; M is the sum of all the edge rights in the network; N is the number of nodes in the system; d_{ij} is the electrical distance between node *i* and node *j*. The Newton-Raphson method is used to calculate the voltage sensitivity of each node, and accordingly the spatial electrical distance. The equation is as follows:

$$d_{ij}=\frac{1}{2}\sum_{k=1}^{N-1}\left[\lg\left|\frac{S_{jk}}{\max\limits_{k} S_{jk}}\right|-\lg\left|\frac{S_{ik}}{\max\limits_{k} S_{ik}}\right|\right]^2 \tag{7}$$

Where: S_{ik} and S_{jk} are the elements of row *i,* column *k*, and row *j,* column *k* of the sensitivity matrix. The voltage sensitivity of each node can be obtained by inverting the Jacobi matrix in the trend calculation; $\max\limits_{k} S_{jk}$ and $\max\limits_{k} S_{ik}$ are the max values of the elements in column *k*.

3.1.2 Functional indicators

In this paper, the functional indicators encompass active power balance, flexibility supply-demand balance, and flexibility probability risk indicators.

(1) Active power balance indicator

In order to quantify the degree of power-load within the VPPs, this paper computes the active power balance indicator using the net load power, as follows:

$$\varphi_{\text{fun}}^{\text{active}}=\frac{1}{S}\sum_{s=1}^{S}\left[1-\frac{1}{T}\sum_{t=1}^{T}\left|\frac{L_{s,t}}{\max\left(L_{s,t}\right)}\right|\right] \tag{8}$$

Where: $\varphi_{\text{fun}}^{\text{active}}$ is the active power balance indicator; S is the total number of clusters; T is the scheduling period; $L_{s,t}$ is the net load power value of cluster *s* at time *t*. If $P_{s,t}<0$, it is represented as the surplus power within the clusters.

(2) Flexibility balance indicators

In order to reflect the ability of VPPs to call upon various types of flexibility resources to meet net load fluctuations on a given time scale, this paper introduces flexibility supply and demand balance indicator and flexibility balance time indicator. The climbing flexibility shortfall is computed, as follows:

$$F_{s,t}^{\tau,+/-}=\begin{cases}\Delta L_{s,t}^{\tau,+/-}-\Delta P_{s,t}^{\tau,+/-},\Delta L_{s,t}^{\tau,+/-}>\Delta P_{s,t}^{\tau,+/-}\\0\qquad\qquad\quad,\Delta L_{s,t}^{\tau,+/-}\le\Delta P_{s,t}^{\tau,+/-}\end{cases}\tag{9}$$

$$\Delta L_{s,t}^{\tau,+/-}=L_{s,t}-L_{s,t+\tau}\tag{10}$$

$$\Delta P_{s,t}^{\tau,+/-}=\Delta P_{AGU,t}^{\tau,+/-}+\Delta P_{AL,t}^{\tau,+/-}+\Delta P_{ESD,t}^{\tau,+/-}\tag{11}$$

Where: $F_{s,t}^{\tau,+/-}$ is the degree of shortage of upward (+) and downward (-) regulation flexibility of cluster *s* at the response time length of τ; $\Delta L_{s,t}^{\tau,+/-}$ is the climbing power of net load at time *t*; $L_{s,t}$ is the net load demand at time *t*; $\Delta P_{s,t}^{\tau,+/-}$ is the climbing power of flexibility that can be provided by cluster *s* at time t; $\Delta P_{AGU,t}^{\tau,+/-}$, $\Delta P_{AL,t}^{\tau,+/-}$ and $\Delta P_{ESD,t}^{\tau,+/-}$ are the climbing power of upward (+) and downward (-) flexibility that can be provided by AGU, AL and ESD at time *t*; τ is the length of response time.

VPPs flexibility climbing power deficit is calculated according to Eq. (11). The flexibility supply-demand balance indicator and the flexibility balance time indicator are calculated separately as follows:

$$\varphi_{\text{fun}}^{\text{flexible}}=1-\frac{1}{S}\sum_{s=1}^{S}\left[\frac{\sum_{t=1}^{T}F_{s,t}^{\tau,+/-}}{\max\left(\sum_{t=1}^{T}F_{s,t}^{\tau,+/-}\right)}\right]\tag{12}$$

$$\varphi_{fun}^{time}=\frac{1}{S}\ \varphi_{fun}^{time}=\frac{1}{S}\sum_{S=1}^{S}[\frac{1}{T}\frac{\sum f_{time}(\triangle L_{s,t}^{\tau,+/-}\le\triangle P_{s,t}^{\tau,+/-})}{\max(\sum_{t=1}^{T}(\triangle L_{s,t}^{\tau,+/-}\le\triangle P_{s,t}^{\tau,+/-})}]\tag{13}$$

Where: $\varphi_{\text{fun}}^{\text{flexible}}$ and $\varphi_{\text{fun}}^{\text{time}}$ are the flexibility supply-demand balance indicator and flexibility balance time indicator; $f_{\text{time}}\left(\Delta L_{s,t}^{\tau,+/-}\le\Delta P_{s,t}^{\tau,+/-}\right)$ is the cumulative time value that satisfies $\Delta L_{s,t}^{\tau,+/-}\le\Delta P_{s,t}^{\tau,+/-}$.

(3) Flexibility probability risk indicator

This paper employs a normal distribution to characterize the probability distribution of the cluster's net load demand according to reference[33], the flexibility probability risk indicator based on conditional probability is introduced, as follows:

$$f_{s,t}^{\tau,+/-}=\begin{cases}\left(\left|L_{s,t+\tau}-L_{s,t}\right|-\Delta P_{s,t}^{\tau,+/-}\right)\times\rho\left(L_{s,t}\right),\Delta L_{s}^{\tau,+/-}\left(t\left|L_{s,t}\right.\right)>\Delta P_{s,t}^{\tau,+/-}\\0\qquad\qquad\qquad\qquad\qquad\qquad,\Delta L_{s}^{\tau,+/-}\left(t\left|L_{s,t}\right.\right)\le\Delta P_{s,t}^{\tau,+/-}\end{cases}\tag{14}$$

$$\varphi_{\text{fun}}^{\text{risk}}=\sum_{s=1}^{S}\frac{\sum_{t=1}^{T}f_{s,t}^{\tau,+/-}}{\max(\sum_{t=1}^{T}f_{s,t}^{\tau,+/-})}\tag{15}$$

Where: $\varphi_{\text{fun}}^{\text{risk}}$ is the flexibility probability risk indicator of the VPPs; $f_{s,t}^{\tau,+/-}$ is the flexibility probabilistic risk indicator of cluster *s* at time *t*; $\Delta L_{s}^{\tau,+/-}\left(t\left|L_{s,t}\right.\right)$ is the net load climbing power of cluster *s* taking into account the uncertainty at time *t*; $\rho\left(L_{s,t}\right)$ is the probabilistic value of $L_{s,t}$ for the value of the net load demand at time *t*.

3.2 Cluster aggregation optimization model

Considering both the structural and functional indicators of cluster aggregation, and treating division method of system as a variable, the VPPs aggregation strategy model is established. The objective is to achieve as much autonomous regulation within each VPP as possible, with the following specific objective functions:

$$\varphi_{\mathrm{VPP}} = \max\left\{\lambda_{\mathrm{str}}\varphi_{\mathrm{str}} + \lambda_{\mathrm{fun}}\left[\left(\varphi_{\mathrm{fun}}^{\mathrm{active}} + \varphi_{\mathrm{fun}}^{\mathrm{time}} + \varphi_{\mathrm{fun}}^{\mathrm{flexible}}\right)\Big/\varphi_{\mathrm{fun}}^{\mathrm{risk}}\right]\right\} \tag{16}$$

Where: φ_{VPP} is the VPPs aggregation target; λ_{str} and λ_{fun} are the weights of structural and functional indicators; The larger λ_{str} is, the more structured the VPPs is and vice versa.

The flexibility provision of VPPs stems from AGU, AL, and ESD. When performing VPPs aggregation, it is necessary to clarify the flexibility capacity that can be provided by different units within the cluster. The specific modeling of flexibility output is as follows:

(1) AGU flexibility output model

For AGU, the flexible regulation output they can provide depends on factors such as the rated capacity of the unit, min technical output, climbing power. They are capable of offering bi-directional regulation capacity, both upward (+) and downward (-), as follows:

$$\Delta P_{AGU,t}^{\tau,+} = \min\left[\Delta R_{AGU,t}^{+} \times \tau, P_{AGU}^{\max} - P_{AGU,t}\right] \tag{17}$$

$$\Delta P_{AGU,t}^{\tau,-} = \min\left[\Delta R_{AGU,t}^{-} \times \tau, P_{AGU,t} - P_{AGU}^{\min}\right] \tag{18}$$

Where: $P_{AGU}^{\max}$ and $P_{AGU}^{\min}$ are the max and min output power of AGU; $\Delta R_{AGU,t}^{+}$ and $\Delta R_{AGU,t}^{-}$ are the upward and downward climbing power of AGU.

(2) ESD flexibility output model

For ESD, the available flexibility to regulate output depends on two factors: charge/discharge power and capacity. It can provide bi-directional regulation capability, both upward (+) and downward (-), as follows:

$$\Delta P_{ESD,t}^{\tau,-} = \min\left\{P_{ESD}^{-,\max}, \left[\left(1 - \mathrm{SOC}_{ESD,t}\right)\eta_{ESD}^{-}\mathrm{C}_{ESD}\right]\Big/\tau\right\} \tag{19}$$

$$\Delta P_{ESD,t}^{\tau,+} = \min\left\{P_{ESD}^{+,\max}, \left[\left(\mathrm{SOC}_{ESD,t} - \mathrm{SOC}_{ESD}^{\min}\right)\eta_{ESD}^{+}\mathrm{C}_{ESD}\right]\Big/\tau\right\} \tag{20}$$

Where: $P_{ESD}^{+,\max}$ and $P_{ESD}^{-,\max}$ are the max ESD charging and discharging power; $\mathrm{SOC}_{ESD}^{\min}$ is the min ESD capacity percentage.

(3) AL flexibility output model

For AL, it offers flexibility to regulate output primarily through two methods: interruptible load and adjustable load. This flexibility can be gauged by the proportion of load that actively participates in demand response, as follows:

$$\Delta P_{AL,t}^{\tau,+/-} = \lambda_{AL,t}^{+/-}\Delta P_{AL,t}^{+/-} \tag{21}$$

$$0 \le \int \lambda_{AL,t}^{+/-}\Delta P_{AL,t}^{+/-} dt \le \Delta L_{AL,t}^{+/-,\max} \tag{22}$$

Where: $\Delta P_{AL,t}^{+/-}$ is the total amount of interruptible and excitable loads at time t; $\lambda_{AL,t}^{+/-}$ is the proportion of interruptible and excitable loads participating in demand response at time t; $\Delta L_{AL,t}^{+/-,\max}$ is the max regulation of interruptible and excitable load.

According to Eq. (16) and Eqs. (17)-(22), the VPPs aggregation strategy model can be established by considering the output limit constraints of Non-AGU, AGU, ESD and AL. According to its own demand, the decision maker adjusts λ_{str} and λ_{fun}, so as to obtain the clusters division scheme that meets the decision maker's needs.

4 Two-stage scheduling optimization model for VPPs

4.1 Cluster scheduling framework system

In order to achieve the optimal operation of VPPs, this paper divides the process into two stages: day-ahead scheduling and real-time balancing. This division is based on the decreasing characteristics of distributed renewable energy power prediction errors with the shortening of the prediction time scale. The cluster scheduling framework system shows in Fig. 2.

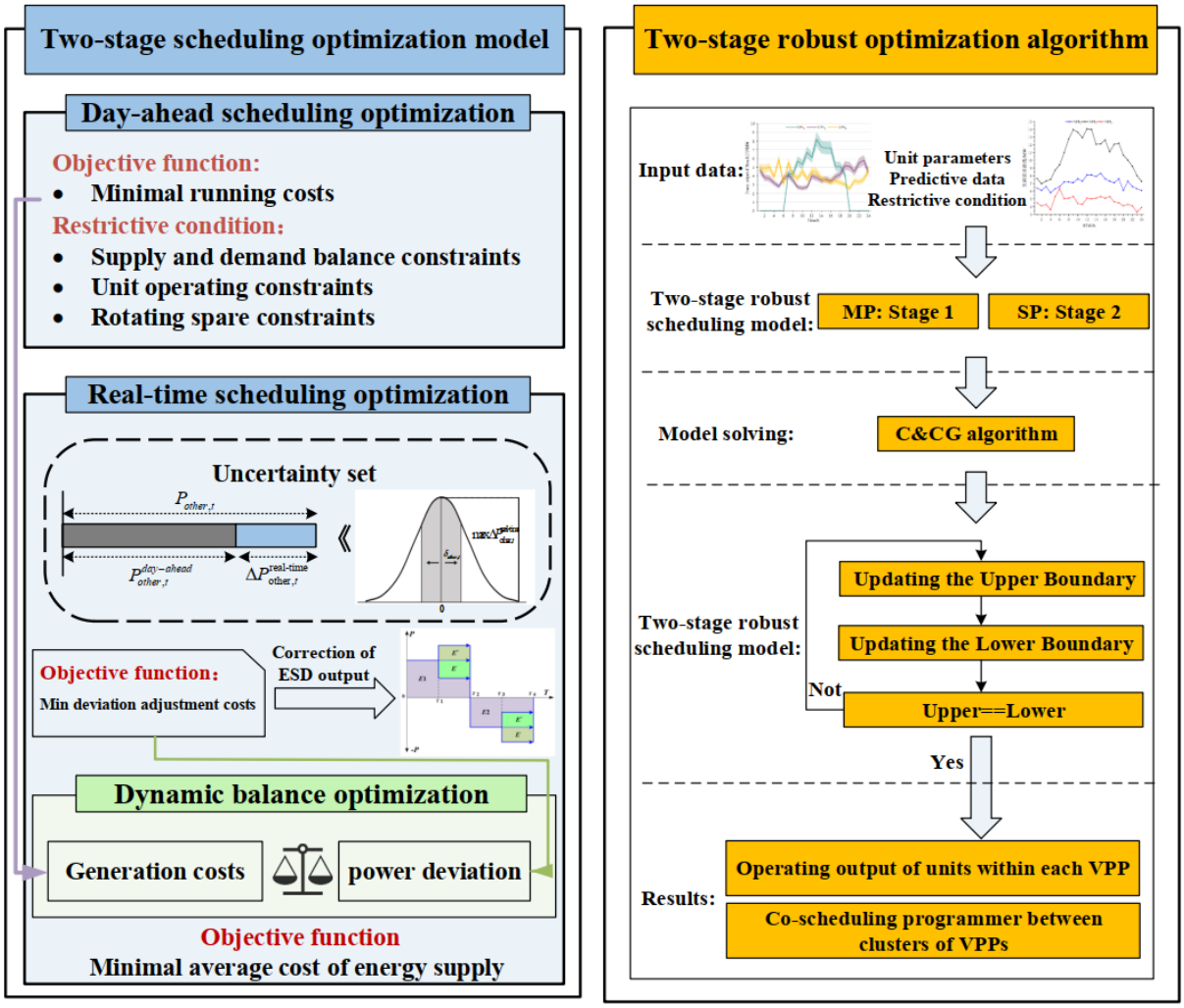

Fig. 2 Two-stage scheduling optimization model for VPP clusters

In the day-ahead stage, the objective is to minimize operating costs, while in the real-time stage, the aim is to minimize adjustment cost. During the real-time stage, each VPP provides data on internal net load fluctuation, real-time generation costs and power deviation to the power system trading center. Each VPP engages in dynamic balance, and the power system trading center optimizes with the objective of minimizing average cost of energy generation. Additionally, considering the influence of balancing power deviation caused by Non-AGU output uncertainty, this paper employs a two-stage robust optimization approach for solving. With the assistance of the C&CG algorithm and strong dyadic theory, the two-stage model is iteratively transformed into the main problem and sub-problems. The two-stage scheduling optimization model for VPP clusters is illustrated in Fig. 2.

4.2 Two-stage cluster scheduling optimization model

4.2.1 Day-ahead power scheduling optimization model

In order to ensure the economy of power system operation, the optimal scheduling strategy for each unit within VPPs needs to be obtained at the day-stage with the minimization of operating cost as the objective function, as follows:

$$\min C_{\mathrm{VPP}}^{\mathrm{cost}}=\sum_{t=1}^{T}\left\{C_{\text{Non-AGU},t}+C_{\mathrm{AGU},t}+C_{\mathrm{ESD},t}+C_{\mathrm{AL},t}+C_{\mathrm{other},t}\right\} \tag{23}$$

$$C_{\mathrm{AGU},t}=\left[a_{\mathrm{AGU}}+b_{\mathrm{AGU}}P_{\mathrm{AGU},t}+c_{AGU}\left(P_{\mathrm{AGU},t}\right)^{2}\right]+$$

$$\left[u_{\mathrm{AGU},t}(1-u_{\mathrm{AGU},t})\right]\times\begin{cases}N_{\mathrm{AGU}}^{hot},T_{\mathrm{AGU}}^{\min}<T_{\mathrm{AGU},t}^{\mathrm{off}}\le T_{\mathrm{AGU}}^{\min}+T_{\mathrm{AGU}}^{cold}\\ N_{\mathrm{AGU}}^{cold},T_{\mathrm{AGU},t}^{\mathrm{off}}>T_{\mathrm{AGU}}^{\min}+T_{\mathrm{AGU}}^{cold}\end{cases} \tag{23a}$$

$$C_{\mathrm{ESD},t}=\frac{\rho_{\mathrm{ESD}}C_{\mathrm{ESD}}^{\mathrm{investmen}}}{N_{\mathrm{ESD}}}+\begin{cases}-c_{\mathrm{ESD}}^{-}\eta_{\mathrm{ESD}}^{-}P_{\mathrm{ESD},t}^{-},P_{ESD,t}^{-}<0\\ c_{\mathrm{ESD}}^{+}\eta_{\mathrm{ESD}}^{+}P_{\mathrm{ESD},t}^{+},P_{ESD,t}^{+}\ge 0\end{cases} \tag{23b}$$

$$C_{\mathrm{AL},t}=P_{AL,t}^{-}c_{AL,t}^{-}+P_{AL,t}^{+}c_{AL,t}^{+} \tag{23c}$$

Where: $F_{\mathrm{VPP}}^{\mathrm{cost}}$ is the operating cost of VPP; $C_{\text{Non-AGU},t}$ is the operating cost of Non-AGU at time *t*, which is taken as the multiplier of generation and unit generation cost; $C_{\mathrm{AGU},t}$, $C_{\mathrm{ESD},t}$ and $C_{\mathrm{AL},t}$ are the operating cost of AGU, ESD and AL at time *t*; $C_{\mathrm{other},t}$ is the cost of power interaction between VPP and other VPPs or the higher level of the grid at time *t*; N_{AGU}^{hot} and N_{AGU}^{cold} are the cost of hot and cold start of AGU; $u_{\mathrm{AGU},t}$ is the operating state of AGU at time *t*; $T_{\mathrm{AGU}}^{\min}$ is the min downtime of AGU; $T_{\mathrm{AGU},t}^{\mathrm{off}}$ and T_{AGU}^{cold} is the min downtime of AGU. ρ_{ESD} is the regulation coefficient; It is introduced in the calculation of the cycle loss cost because the output of the battery in each scheduling period is only half process of charging or discharging; $C_{\mathrm{ESD}}^{\mathrm{investmen}}$ is the initial investment cost of the battery; N_{ESD} is the service life of the battery; c_{ESD}^{-} and c_{ESD}^{+} are the cost of charging and discharging loss of the ESD; $c_{AL,t}^{-}$ and $c_{AL,t}^{+}$ are the cost of scheduling of the interruptible loads and the excitable loads at time *t*.

Comprehensive consideration of power balance constraints, unit operation constraints and AL output constraints is necessary when conducting VPP multi-objective optimization, as detailed below:

(1) Electricity balance constraints

$$P_{\text{Non-AGU},t}+P_{\mathrm{AGU},t}\left(1-\alpha_{\mathrm{AGU}}\right)+P_{\mathrm{ESD},t}^{+}\left(1-\eta_{\mathrm{ESD}}^{+}\right)+\Delta P_{AL,t}^{+}+P_{\mathrm{other},t}=L_{VPP,t}+P_{ESD,t}^{-}\left(1-\eta_{ESD}^{-}\right)+\Delta P_{AL,t}^{-} \tag{24}$$

Where: $L_{VPP,t}$ is the load demand inside VPP at time *t* ; α_{AGU} is the generation loss rate of AGU at time *t*; $P_{\mathrm{other},t}$ is the amount of power interacting between VPP and the outside at time *t*.

(2) Non-AGU and AGU operational constraints

Within VPPs, there are two types of units: Non-AGU and AGU. Each unit's generation outputs fall within the min and max output thresholds. Additionally, for AGU units, considerations include climb constraints and time constraints, as follows:

$$u_{\mathrm{AGU},t}\Delta P_{\mathrm{AGU},t}^{-}\le P_{\mathrm{AGU},t}-P_{\mathrm{AGU},t-1}\le u_{\mathrm{AGU},t}\Delta P_{\mathrm{AGU},t}^{+} \tag{25}$$

$$\left(T_{\mathrm{AGU},t\text{-}1}^{\mathrm{on}}-M_{\mathrm{AGU}}^{\mathrm{on}}\right)\left(u_{\mathrm{AGU},t\text{-}1}-u_{\mathrm{AGU},t}\right)\ge 0 \tag{26a}$$

$$\left(T_{\mathrm{AGU},t\text{-}1}^{\mathrm{off}}-M_{\mathrm{AGU},t}^{\mathrm{off}}\right)\left(u_{\mathrm{AGU},t}-u_{\mathrm{AGU},t\text{-}1}\right)\ge 0 \tag{26b}$$

Where: $\Delta P_{\mathrm{AGU},t}^{+}$ and $\Delta P_{\mathrm{AGU},t}^{-}$ are the up and down climbing power of AGU at time *t*; $T_{\mathrm{AGU},t\text{-}1}^{\mathrm{on}}$ and

$T_{\mathrm{AGU},t\text{-}1}^{\mathrm{off}}$ are the continuous startup and shutdown time of AGU at time t-1; $M_{\mathrm{AGU}}^{\mathrm{on}}$ and $M_{\mathrm{AGU},t}^{\mathrm{off}}$ are the min startup and shutdown time allowed by AGU.

(3) ESD operational constraints

ESD operation constraints include battery power constraints and charge/discharge power constraints. In order to analyze ESD battery power state, State of Charge (SOC) is introduced to reflect the residual power of ESD battery. SOC is expressed as a percentage of the battery's residual power and its total capacity, as follows:

When ESD is in the charging state:

$$\mathrm{SOC}_{ESD,t} = \mathrm{SOC}_{ESD,t\text{-}1} + \left(1\text{-}\eta_{ESD}^{-}\right) P_{ESD,t}^{-} \Big/ \mathrm{C}_{ESD} \tag{27a}$$

When ESD is in the discharging state:

$$\mathrm{SOC}_{ESD,t} = \mathrm{SOC}_{ESD,t\text{-}1} - P_{ESD,t}^{+} \Big/ \left[\left(1\text{-}\eta_{ESD}^{+}\right)\mathrm{C}_{ESD}\right] \tag{27b}$$

Where: $\mathrm{SOC}_{ESD,t}$ and $\mathrm{SOC}_{ESD,t\text{-}1}$ are the remaining battery charge of ESD at time t and t-1, the max value is 100%; C_{ESD} is the rated capacity of ESD battery.

(4) AL output constraints

For AL, the output methods include interruptible and excitable methods, which need to satisfy the min and max output constraints. In order to avoid over-response that leads to peak and valley inversion of the load curve, it also needs to satisfy the max response amount constraints, as follows:

$$\sum_{t=1}^{T} \Delta P_{AL,t} \le \Delta P_{AL}^{\max} \tag{28a}$$

$$\left[\eta_{\mathrm{off}},\ \eta_{\mathrm{on}}\right] = \begin{cases} \left[1,0\right], P_{\mathrm{AGU}} - L_{VPP} \ge \Delta P_{AL,t}^{+} \\ \left[0,1\right], L_{VPP} - P_{\mathrm{AGU}} \ge \Delta P_{AL,t}^{-} \\ \left[0,0\right], \mathrm{other} \end{cases} \tag{28b}$$

Where: $\Delta P_{AL}^{\max}$ is the max output that can be provided by AL; P_{AGU} and L_{VPP} are the total output and total load demand of VPP.

(5) Rotating standby constraints

$$P_{VPP,t}^{\max} - P_{VPP,t} + P_{AL,t}^{+} + \left(P_{ESD}^{+,\max} \text{-} P_{ESD,t}^{+,}\right) \ge r_1 L_{VPP,t} + r_2 P_{WPP,t} + r_3 P_{PV,t} \tag{29a}$$

$$P_{VPP,t} - P_{VPP,t}^{\min} + P_{AL,t}^{-} + \left(P_{ESD}^{-} \text{-} P_{ESD,t}^{-,\min}\right) \ge r_4 \cdot P_{WPP,t} + r_5 \cdot P_{PV,t} \tag{29b}$$

Where: $P_{VPP,t}^{\max}$ and $P_{VPP,t}^{\min}$ are the max and min available output of VPP at time t; $P_{VPP,t}$ is the generation output of VPP at time t; r_1 r_2 and r_3 are the upper rotating reserve factors of load, WPP and PV; r_4 and r_5 are the lower rotating reserve factors of WPP and PV; $P_{ESD}^{+,\max}$ is the max discharge power of ESD; $P_{ESD}^{-,\min}$ is the min charge power of ESD.

4.2.2 Real-time balanced scheduling optimization model

Given that each VPP manages its own internal power supply and demand balance, this section delves into uncovering the complementary characteristics among different VPPs. A VPPs cooperative scheduling optimization model are established.

4.2.2.1 Uncertainty variable set construction

Given the significant uncertainty in the generation output of Non-AGU, day-ahead scheduling strategy may deviate in the real-time stage. Consequently, the balanced power $P_{\mathrm{other},t}$ required by VPP to meet its power demand becomes an uncertain variable. Capturing the impact of this uncertainty on the VPPs scheduling plan is crucial in formulating the optimal VPPs scheduling strategy. To address this, $P_{\mathrm{other},t}$ is divided into

deterministic and uncertain components, as follows:

$$P_{\text{other},t}=P_{\text{other},t}^{\text{day-ahead}}+\Delta P_{\text{other},t}^{\text{real-time}} \tag{30}$$

Where: $P_{\text{other},t}^{\text{day-ahead}}$ is the equilibrium power of VPP in the day-ahead stage. $\Delta P_{\text{other},t}^{\text{real-time}}$ is the balanced power of the deviation of the real-time stage. Set the deviation value of this variable obeys the normal distribution $\Delta P_{\text{other},t}^{\text{real-time}} \sim \left[0,\delta_{\text{other},t}\right]$. Then $P_{\text{other},t}$ obeys the normal distribution $P_{\text{other},t} \sim \left[P_{\text{other},t}^{\text{day-ahead}},\delta_{RE,t}^{2}\right]$. Set the confidence level β , and get the max fluctuation range of the stochastic scenario $\Delta P_{\text{other},t}^{\text{real-time}}$ under the confidence level β as follows:

$$\Delta \hat{P}_{\text{other},t}^{\text{real-time}}=\max\left\{\left(P_{\text{other},j,t}-P_{\text{other},t}\right),j\subset J\right\} \tag{31}$$

According to Eq. (31), the max fluctuation value of the required balancing power of VPP is obtained, and further, its uncertainty is expressed as an uncertainty set U. The procedure is as follows:

$$U=\left\{\begin{array}{l}\boldsymbol{P}_{\text{other}}\in\boldsymbol{R}^{T\times T}:\sum_{t=1}^{T}\left|P_{\text{other},t}-P_{\text{other},t}^{\text{day-ahead}}\right|\Big/\Delta\hat{P}_{\text{other},t}^{\text{real-time}}\le\Gamma,\\ P_{\text{other},t}^{\text{day-ahead}}-\Gamma\Delta\hat{P}_{\text{other},t}^{\text{real-time}}\le P_{\text{other},t}\le P_{\text{other},t}^{\text{day-ahead}}+\Gamma\Delta\hat{P}_{\text{other},t}^{\text{real-time}}\end{array}\right\} \tag{32}$$

Where: $\boldsymbol{P}_{\text{other}}$ is the vector form of the balancing power required by VPP; Γ is the uncertainty margin of the balancing power required by VPP, which is used to regulate the conservatism of the uncertainty set. The larger the value means the higher the degree of fluctuation is, and the more robust the scheduling result is obtained.

4.2.2.2 Multi-VPP balanced scheduling optimization model

In the real-time stage, due to the strong uncertainty of Non-AGU, AGU, ESD and AL need to be invoked to provide flexible output when the prediction value of the day-ahead deviates from the actual value. So the objective is to minimize the deviation of the output of each unit as follows:

$$\min C_{VPP}^{adjust}=\sum_{t=1}^{T}\eta_{\gamma}\left|\Delta P_{\gamma,t}\right| \tag{33}$$

Where: C_{VPP}^{adjust} is the cumulative output deviation variance of VPP; γ is AGU, ESD, and AL ; η_{γ} is the unit adjustment cost of each unit; $\Delta P_{\gamma,t}$ is the adjustment output of each unit in the real-time stage.

When Non-AGU output deviates, the output deviation is balanced by amending ESD output plan. At the same time, the correction of ESD operating output should not affect ESD planned operating output at the next moment. Consequently, ESD constraint is as follows:

$$\text{SOC}_{ESD,t}^{real-time}=\begin{cases}\text{SOC}_{ESD,t-1}^{real-time}+\left(1\text{-}\eta_{ESD}^{-}\right)P_{ESD,t}^{-}\Big/\text{C}_{ESD}\\ \text{SOC}_{ESD,t-1}^{real-time}-P_{ESD,t}^{+}\Big/\left[\left(1\text{-}\eta_{ESD}^{+}\right)\text{C}_{ESD}\right]\end{cases} \tag{34}$$

Similarly, the corrected ESD operating output, which also adhere to the constraints of Eq. (24), Eq. (29b) and Eq. (33). Consequently, a corrected plan for real-time scheduling of VPPs with different robustness coefficients is obtained. Further, the residual power supply capacity of each VPP can be calculated as follows:

$$\Delta P_{VPP,t}=\left\{\begin{array}{ll}\min\left\{\Delta P_{\text{AGU},t}^{+},\left(g_{\text{AGU}}^{\max}-g_{\text{AGU},t}^{real-time}\right)\right\}+\min\left\{S_{ESD,t},\left(P_{ESD}^{+,\max}\text{-}P_{ESD,t}^{+,\text{real-time}}\right)\right\} & ,P_{other,t}>0\\ \min\left\{\Delta P_{\text{AGU},t}^{+},\left(g_{\text{AGU}}^{\max}-g_{\text{AGU},t}^{real-time}\right)\right\}+\min\left\{S_{ESD,t},\left(P_{ESD}^{+,\max}\text{-}P_{ESD,t}^{+,\text{real-time}}\right)\right\}+P_{other,t} & ,P_{other,t}\le 0\end{array}\right\} \tag{35}$$

Where: $\Delta P_{VPP,t}$ is the generation output of VPP that can participate in the balancing market at time *t*; $P_{\text{WPP},t}^{\text{real-time}}$, $P_{\text{PV},t}^{\text{real-time}}$ and $P_{ESD,t}^{+,\text{real-time}}$ are the generation output of WPP, PV and ESD in the real-time stage at time *t*;

$P_{\mathrm{WPP},t}^{\text{day-ahead}}$, $P_{\mathrm{PV},t}^{\text{day-ahead}}$ and $g_{\mathrm{AGU},t}^{\text{day-ahead}}$ are the generation output of WPP, PV and AGU in the day-ahead stage at time *t*.

Additionally, generation costs of each VPP can be calculated using Eqs. (23) and (33). The load demand of each VPP can be determined based on the day-ahead and real-time scheduling strategy. From this, the average generation costs reported to the control center can be computed as follows:

$$B_{VPP,t} = \left(1+\beta_{VPP,t}\right) F_{\mathrm{VPP}}^{\mathrm{cost}} \Big/ L_{VPP,t} \tag{36}$$

The total costs and residual power supply capacity of VPPs are determined by Eq.(23), Eq. (33) and Eq. (35). In systems with VPP clusters, the control center categorizes each VPP into a supplying side or a receiving side based on the reported deviation power of each VPP. Subsequently, the control center executes energy transfers according to the order of average energy generation cost, from highest to lowest, until energy balance is achieved. Each time period each VPP interacts with the information process of independently reporting its own average cost of supply and deviation power. This paper introduces the function argmax g (•), which denotes a set of solution sets within the domain of definition. Each set of solutions can maximize the function argmax g (•). Consequently, the optimal strategies for multiple VPPs in receiving instructions from the control center for balanced scheduling are as follows:

$$\begin{cases} \boldsymbol{B}_1^* \in \arg\max\left[\left(\boldsymbol{B}_1 \text{-} \boldsymbol{C}_1\right)\cdot \boldsymbol{E}_1\left(\boldsymbol{B}_1, \boldsymbol{B}_2^*, \cdots, \boldsymbol{B}_m^*\right)\right] \\ \boldsymbol{B}_2^* \in \arg\max\left[\left(\boldsymbol{B}_2 \text{-} \boldsymbol{C}_2\right)\cdot \boldsymbol{E}_2\left(\boldsymbol{B}_1^*, \boldsymbol{B}_2, \cdots, \boldsymbol{B}_m^*\right)\right] \\ \vdots \\ \boldsymbol{B}_m^* \in \arg\max\left[\left(\boldsymbol{B}_m \text{-} \boldsymbol{C}_m\right)\cdot \boldsymbol{E}_m\left(\boldsymbol{B}_1^*, \boldsymbol{B}_2^*, \cdots, \boldsymbol{B}_m\right)\right] \end{cases} \tag{37}$$

Where: *m* is VPP number; $\boldsymbol{B}_m$ is the energy supply strategy of VPP$_m$; $\boldsymbol{B}_m^*$ is the final energy supply strategy of VPP$_m$; $\boldsymbol{E}_m\left(\boldsymbol{B}_1^*, \boldsymbol{B}_2^*, \cdots, \boldsymbol{B}_m\right)$ is the final energy supply scheme after balanced scheduling of VPP_m control centre.

According to Eq. (32), to analyse the impact of uncertainty on the dynamic balancing strategy of VPP clusters, this paper introduces a two-stage robust optimization method. This method takes the lowest average generation cost as the optimization objective. The specific objective function as follows:

$$\max_{U}\min_{\Omega} \; F_{\mathrm{Bidding}} = \sum_{t=1}^{T}\sum_{m=1}^{M}\left\{\left[\left(\boldsymbol{B}_m^* \text{-} \boldsymbol{C}_m\right)\cdot \boldsymbol{E}_m\left(\boldsymbol{B}_1^*, \boldsymbol{B}_2^*, \cdots, \boldsymbol{B}_m\right)\right]_t \Big/ \sum_{m=1}^{M} \boldsymbol{E}_m\left(\boldsymbol{B}_1^*, \boldsymbol{B}_2^*, \cdots, \boldsymbol{B}_m^*\right)_t\right\} \tag{38}$$

$$\sum_{m=1,\, m\neq n}^{M} \Delta P_{\mathrm{VPP},t}^{m\text{-}n} + P_{\mathrm{grid},t}^{n} = P_{\mathrm{other},t}^{n} \tag{39a}$$

$$\left|\Delta P_{\mathrm{VPP},t}^{m\text{-}n}\right| \le \Delta P_{\mathrm{VPP},t}^{m\text{-}n,\max} \tag{39b}$$

Where: $\Delta P_{\mathrm{VPP},t}^{m\text{-}n}$ is the generation output supplied by VPP$_m$ to VPP$_n$ at time *t*; $\Delta P_{\mathrm{VPP},t}^{m\text{-}n,\max}$ is the max generation output that VPP$_m$ can provide to VPP$_n$ at time *t*; $P_{\mathrm{grid},t}^{n}$ is the amount of power purchased by VPP$_n$ from the higher-level grid at time *t*; $P_{\mathrm{other},t}^{n}$ is the amount of balancing power required by VPP$_n$ at time *t*.

4.3 Two-stage scheduling model solution

The two-stage robust scheduling optimization model proposed in this paper is in the form of min-max-min three-layer optimization. The common solution paths are Benders decomposition and C&CG algorithm. Specifically, the original problem is decomposed into the master problem and sub-problems in a max-min format. Through the Karush-Kuhn-Tucker (KKT) condition or Strong Duality Theory (SDT), the problem is transformed into a single-layer optimization model. Subsequently, the master-subproblem is iterated to obtain the optimal solution for the original problem. Previous studies [34] have confirmed that the C&CG algorithm

exhibits higher solution efficiency compared to the Benders decomposition method. Therefore, in this paper, the C&CG algorithm is employed to solve the VPPs scheduling optimization model, and Eq. (38) is rewritten as follows:

$$\min_{\boldsymbol{x}_1\in\boldsymbol{\Omega}_1}\left(\boldsymbol{c}_1\right)^T\boldsymbol{x}_1+\max_{P_{\text{other},t}\in\boldsymbol{U}}\left(\boldsymbol{b}^T P^2_{\text{other},t}+\min_{\boldsymbol{x}_2\in\boldsymbol{\Omega}_2}\left(\boldsymbol{c}_2\right)^T\boldsymbol{x}_2\right)$$

$$s.t.\begin{cases}\boldsymbol{\Omega}_1=\left\{\boldsymbol{x}_1\middle|\,\boldsymbol{A}\boldsymbol{x}_1\le\boldsymbol{a}\right\}\\ \boldsymbol{U}=\left\{\begin{array}{l}\boldsymbol{P}_{\text{other}}\in\boldsymbol{R}^{T\times T}:\sum_{t=1}^{T}\left|P_{\text{other},t}-P^{\text{day-ahead}}_{\text{other},t}\right|\Big/\Delta\hat{P}^{\text{real-time}}_{\text{other},t}\le\Gamma,\\ P^{\text{day-ahead}}_{\text{other},t}-\Gamma\Delta\hat{P}^{\text{real-time}}_{\text{other},t}\le P_{\text{other},t}\le P^{\text{day-ahead}}_{\text{other},t}+\Gamma\Delta\hat{P}^{\text{real-time}}_{\text{other},t}\end{array}\right\}\\ \boldsymbol{\Omega}_2=\left\{\boldsymbol{x}_2\middle|\,\boldsymbol{D}\boldsymbol{x}_2\le\boldsymbol{E}\boldsymbol{x}_1+\boldsymbol{F}P^1_{\text{other},t}+\boldsymbol{d}\right\}\end{cases}\tag{40}$$

Where: $\boldsymbol{x}_1$ is the decision variable of stage 1; $\boldsymbol{x}_2$ is the decision variable of stage 2; $P^1_{\text{other},t}$ and $P^2_{\text{other},t}$ are the VPP equilibrium power in stage 1 and stage 2; $\boldsymbol{c}_1$, $\boldsymbol{b}$, $\boldsymbol{c}_2$, $\boldsymbol{A}$, $\boldsymbol{a}$, $\boldsymbol{D}$, $\boldsymbol{E}$, $\boldsymbol{F}$ and $\boldsymbol{d}$ are the constant matrices of objective function and constraints.

According to Eq. (40), the C&CG algorithm is used to solve the three-layer robust optimization problem by subproblem iteration. This process primarily involves transforming the original problem into a first-stage master problem and a second-stage subproblem. The main problem encompasses the first-stage model and subproblem to identify the worst-case scenario of each unit's output constraints. Meanwhile, the subproblem constitutes a two-layer max-min optimization problem, which can be converted into a maximization problem using SDT of the inner minimization problem. After transformation, the subproblem model is iteratively solved. The specific model transformation is delineated in the appendix.

According to Eq. (40), the master subproblem is solved using the C&CG algorithm as follows:

Step 1: Initialize variables and assign initial values. Set the number of iterations *i*=1, the upper bound of the objective function $U_B\to+\infty$, the lower bound as $L_B\to+\infty$. Additionally, set convergence judgement coefficients ε, ε to be sufficiently small values greater than zero;

Step 2: Solve the main problem by employing the appendix Eq. (1). Obtain the objective function value V_i and control variables $\boldsymbol{x}_{1,i}$. Update the lower bound of the objective function to $L_B=V_i$;

Step 3: Solve the subproblem by employing the appendix Eq. (2). Obtain the objective function value f_i and the worst-case operating scenario value $\boldsymbol{g}^{2*}_{RE,k}$. Return the constraints in the appendix Eq. (2) to the main problem of Eq. (40). Updating the upper bound of the objective function to $U_B=\min\left\{U_B,\left(\boldsymbol{c}_1\right)^T\boldsymbol{x}_{1,k}+f_i\right\}$;

Step 4: Determine convergence. If $\left(U_B-L_B\right)\big/L_B\le\varepsilon$, the problem converges and the iteration stops. The objective function value is U_B; Otherwise, continue the iteration, *i* = *i* + 1, return to step 2.

5 Synergistic benefit allocation strategy of VPPs

5.1 Shapley value method

The Shapley value method stands as a classical algorithm designed to resolve multi-member cooperative game problems. This method determines the benefits shared by all members within the coalition by computing the expected value of their marginal contributions. By allocating benefits based on the Shapley value, the method accurately reflects each member's degree of contribution to the coalition's overall goal, thereby sidestepping egalitarianism in distribution. Furthermore, it mirrors the process of mutual games among

coalition members. For the cooperative coalition $N:\{(1,2,\ldots,N)\}$ consisting of U members, define S as a subset of N. If $V(\varphi)=0$, φ is the empty set, $V(S_1 \cup S_2) \geq V(S_1)+V(S_2)$, and satisfies $S_1 \cup S_2=\varphi$. Here, $[N, V]$ is termed the cooperative game strategy of the *nth* member. Consequently, the benefit allocation schemes of different members are derived as follows:

$$V_i = \sum_{S_i \subseteq S} \frac{(|S|-1)!(N-|S|)!}{|N|!}\left(v(S)-v(S/i)\right) \tag{41}$$

Where: V is the characteristic function of the co-operative alliance. It meaning is the profit gained from the co-operation of the alliance under different alliance membership compositions; S_i is all the subsets containing element i; $|S|$ is the number of elements in the subset S; $v(S)$ is the profit of the co-operation of the alliance containing element i; $v(S/i)$ is the profit of the co-operation of the alliance not containing element i.

5.2 Improvement of the two-layer benefit allocation method

The aggregation scheduling of VPPs involves two layers: optimization within individual VPP and co-scheduling between them. However, conventional Shapley value method fails to differentiate between the operational optimization objectives of these layers during benefit allocation. To address this limitation, this paper extends the Shapley value method into a two-layer benefit allocation approach. Fig. 3 illustrates the framework for two-layer benefit allocation in VPPs.

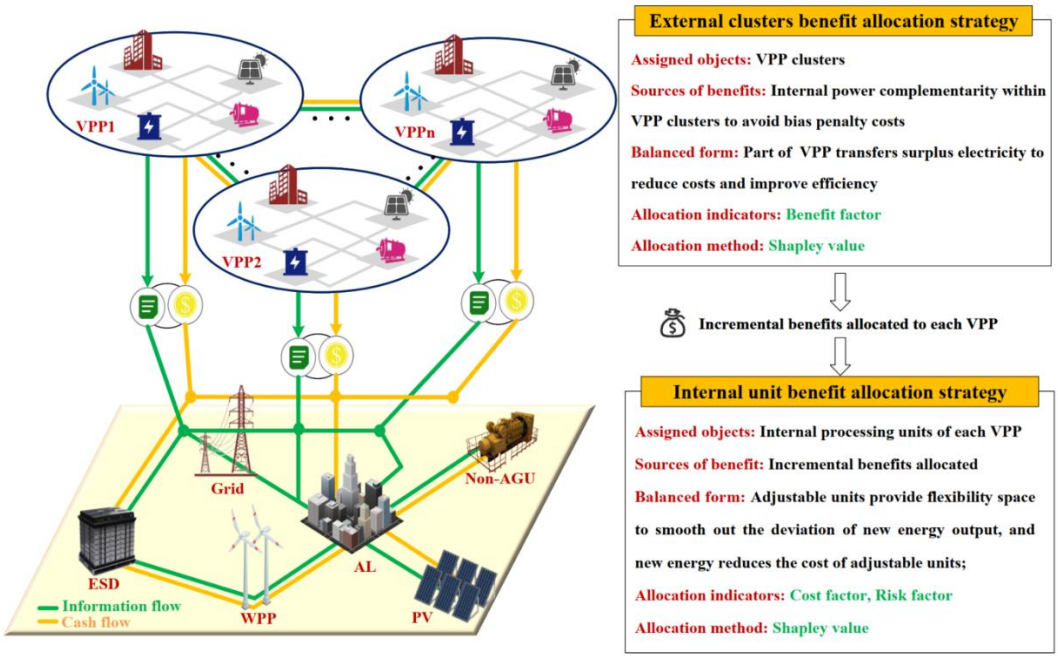

Fig. 2 The framework for two-layer benefit allocation in VPPs

According to Fig. 3 and the two-stage scheduling optimization model for VPPs in Section 4, this paper presents a two-layer benefit allocation method for VPPs. In VPPs, owing to their energy complementarity during the real-time stage, they can circumvent deviation penalty costs, resulting in increased benefits. To account for this, a benefit factor is introduced to facilitate equitable benefit allocation. Additionally, given the significant disparities in risk and cost contributions among different types of units within VPP, this paper incorporates risk and cost factors for internal benefit allocation. This approach ensures the fairness of benefit allocation while enhancing the participation willingness of distributed energy resources in VPP.

5.2.1 External cluster benefit allocation strategy

The VPPs formulates an optimal scheduling strategy by leveraging the power complementarity across different VPPs. During this process, part of VPPs purchase excess power from others to uphold supply-demand equilibrium and evade deviation penalty costs, while others may sell surplus power to augment operational revenue. It can be seen that the VPP clusters scheduling revenue is higher than the revenue sum of independent scheduling of each VPP, which meets the allocation requirements of the Shapley value method. The benefit factor is introduced as the external cluster benefit allocation indicator, calculated as follows:

$$\Delta R_{VPP,s} = \sum_{t=1}^{T} \left(P_{VPP,s,t}^{\text{output}} B_{VPP,s,t}^{\text{output}} - P_{VPP,s,t}^{\text{input}} B_{VPP,s,t}^{\text{input}} \right) \tag{42}$$

$$R_s = \sum_{U_s \subseteq U} \frac{\left(|U|-1\right)!\left(M-|U|\right)!}{|M|!} \left[\Delta R_{VPP}\left(U\right) \text{-} \Delta R_{VPP,s}\left(U/s\right) \right] \tag{43}$$

Where: $\Delta R_{VPP,s}$ is the incremental benefit of VPP*s* participating in cluster scheduling; $P_{VPP,s,t}^{\text{input}}$ and $P_{VPP,s,t}^{\text{output}}$ are the input and output power of VPP*s* at time *t*; $B_{VPP,s,t}^{\text{input}}$ and $B_{VPP,s,t}^{\text{output}}$ are the input and output power price of VPP*s* at time *t* ; $\Delta R_{VPP}\left(U\right)$ is the eigenfunction of incremental benefit of VPPs; U is the VPPs alliance; R_s is the benefit allocation coefficient of VPP*s*.

5.2.2 Internal unit benefit allocation strategy

Within each VPP, there are four types of entities: Non-AGU, AGU, ESD, and AL. Given the strong uncertainty associated with Non-AGU, it becomes imperative to mobilize AGU, ESD, and AL to furnish flexible output, achieving optimal power equilibrium. Hence, the cost factor and risk factor, derived from Eq. (23) and Eq. (33), are introduced as indices for internal unit benefit allocation. The cost and risk factors are calculated as follows:

$$C_i = \sum_{U_{\text{VPP},i} \subseteq U_{\text{VPP}}} \frac{\left(\left|U_{\text{VPP}}\right|-1\right)!\left(I-\left|U_{\text{VPP}}\right|\right)!}{|I|!} \left[C_{\text{VPP}}^{\text{cost}}\left(U_{\text{VPP}}\right) - C_{\text{VPP}}^{\text{cost}}\left(U_{\text{VPP}}/i\right) \right] \tag{44}$$

$$C_{VPP} = C_{VPP}^{cost} + C_{VPP}^{adjust} \tag{44a}$$

$$F_i = \sum_{U_{\text{VPP},i} \subseteq U_{\text{VPP}}} \frac{\left(\left|U_{\text{VPP}}\right|-1\right)!\left(I-\left|U_{\text{VPP}}\right|\right)!}{|I|!} \left[F_{VPP}^{adjust}\left(U_{\text{VPP}}\right) \text{-} F_{VPP}^{adjust}\left(U_{\text{VPP}}/i\right) \right] \tag{45}$$

$$F_{VPP}^{adjust} = \sum_{t=1}^{T} (\Delta P_{m,t})^2 \tag{45a}$$

Where: C_i and F_i are the cost and risk factor of VPP internal unit *i*; U_{VPP} is the VPP internal unit alliance; I is the number of VPP internal units; *m* is Non-AGU, AGU, ESD, and AL.

5.3 Composite benefit allocation factor

Based on the benefit allocation shares for each virtual power plant derived from Eq. (43), alongside the cost factor and risk factor for each unit within VPP established by Eq. (44) and Eq. (45), the composite benefit allocation factor for different VPPs is computed as follows:

$$R_i = \lambda_i C_i \Big/ \sum_{i \in I} C_i + \left(1\text{-}\lambda_i\right) F_i \Big/ \sum_{i \in I} F_i, \quad \forall \text{VPP } s \tag{46}$$

$$R_{s,i} = \left[R_i\right]_s \times R_s \tag{47}$$

Where: $R_{s,i}$ is the benefit allocation factor of unit *i* within VPP*s*; R_i is the benefit allocation factor of unit *i* within VPP*s*; λ_i is the cost factor weight of unit *i* within VPP*s*.

6 Example analysis

6.1 Basic data

Huangyuan County, situated in the western part of Qinghai Lake within Xining City, Qinghai Province, boasts rich light and abundant water, alongside favorable wind conditions, granting it significant energy resource advantages. As a national ecological civilisation construction demonstration county, the renewable energy installed capacity accounted for more than 60% and 90%, ranked among the forefront in China. In this section, the 10kV distribution network in Huangyuan County is taken as an example. The topology is shown in Fig. 4 to demonstrate the effectiveness of the VPPs segmentation, the two-stage scheduling optimization, and the effectiveness of the benefit allocation strategy.

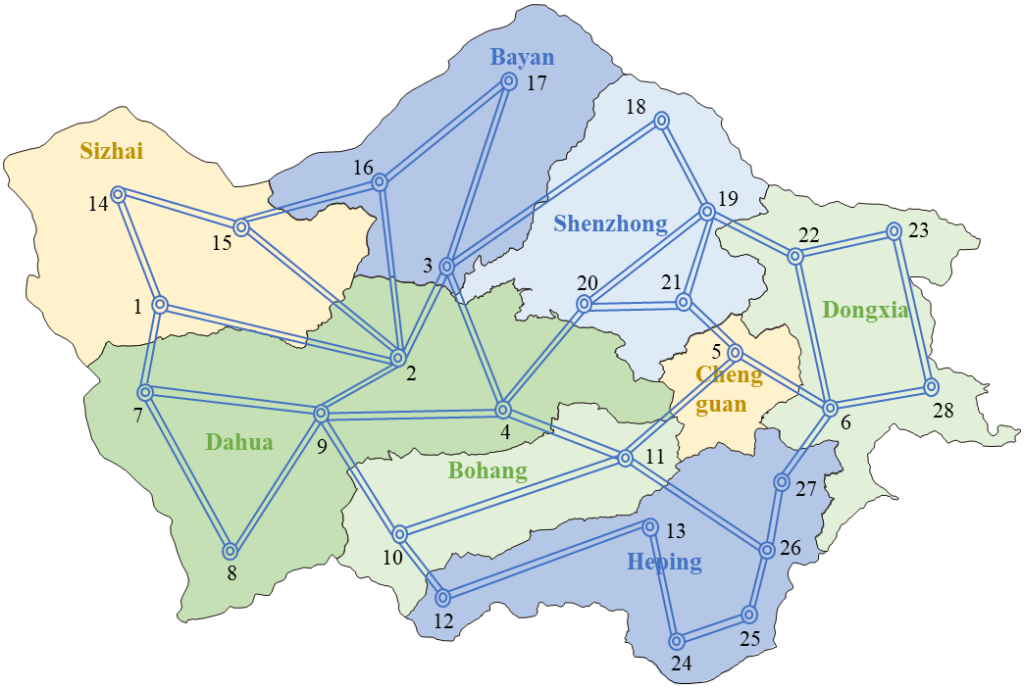

Fig.3 Actual distribution system structure in Huangyuan County

There are 28 nodes in this distribution network system, including 16 Non-AGU nodes (9 WPP nodes and 7 PV nodes), 3 AGU nodes, 3 ESD nodes and 6 AL nodes. The capacity configurations and parameters of the system units are set as follows: WPP units are located at nodes 7, 8, 11, 12, 13, 24, 26, 27, and 28, where nodes 7, 8, and 11 have the rated power of 1 MW and the max output power of 1.5 MW. Nodes 12, 13, 24, 26, 27, and 28 have the rated power of 0.8 MW and the max output power of 1MW. PV are located at 14, 15, 16, 17, 18, 19 and 20, with unit rated power of 0.8MW and max output power of 1.2MW; AGU are set at nodes 2, 3 and 5, with max output power of 2MW, 4MW and 5MW, and rated output power of 1MW, 2MW, and 3.5MW. The start-stop cost of AGU is 1000¥ once, the climbing rate is 0.5MW/h, 1MW/h, 1.75MW/h, and the min output power is 1MW; ESD are set at nodes 1, 6, and 10, the max storage capacity is 10MWh, the min storage capacity is 1MWh, the initial capacity is 4MWh, the max charging power is 1.5 MW/h, and the max discharge power is 2MW/h. AL are set at 4, 9, 20, 22, 23, and 25, where the interruptible loads are located at 4, 20, and 23, and the incentivisable loads are located at 9, 22, and 25. The cost of the demand response is 400¥/MW, and the max control of the nodes of the interruptible loads and the incentivisable loads is 10% of the load.

In this paper, the analysis focuses on the typical day scenario of each node, spanning a simulation time of 24 hours, with the results depicted in Fig. 5. The resistance parameters of each feeder in the distribution

network are selected based on the line impedance, utilizing Matpower to establish a trend model. This model facilitates the extraction of the reactive voltage sensitivity matrix of the network. Subsequently, the electrical distance of each node is calculated and normalized. The normalized electrical distances of each node are illustrated in Fig. 6.

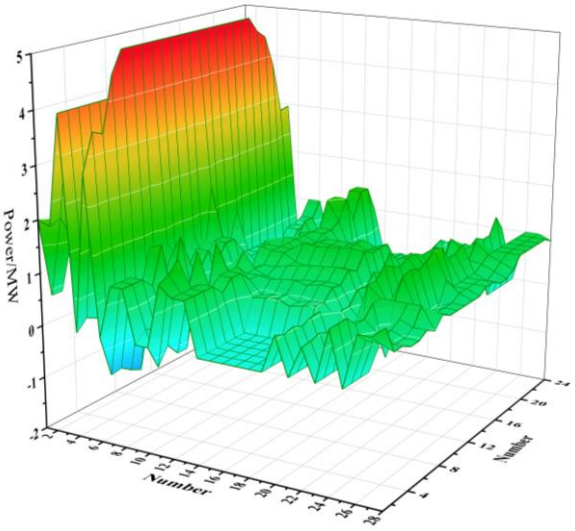

Fig. 5 Typical daily scenario data

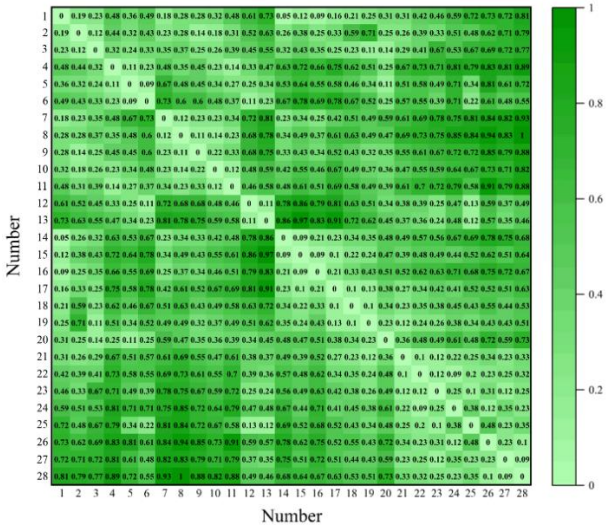

Fig. 6 Electrical distance data after normalisation

In this study, the fuel cost curve of AGU is linearized into two segments, with slope coefficients of 110¥/MW and 362¥/MW, respectively. Parameter settings for the remaining distributed energy units are provided in Table 1. MATLAB 2018b and Pycharm are utilized in this paper for programming virtual power plant cluster division, two-stage scheduling optimization, and benefit allocation.

Table 1 Distributed energy device parameter settings

character	Value	character	Value
α_{MT}	0.2	r_1	0.1
C_{ESS}^{+}	300¥/MW	r_2	0.1
C_{ESS}^{-}	300¥/MW	r_3	0.1
η_{ESS}	0.95	r_4	0.2
C_{other}	800¥/MW	r_5	0.2

6.2 Example results

6.2.1 VPPs segmentation results

Firstly, the structural indicator φ_{str} and functional indicator φ_{fun} are used to construct the optimal objective of node system cluster division. Since the application of multi-indicator cluster division constitutes a multi-objective optimization problem, achieving optimal results for all objectives simultaneously is difficult. Therefore, in this paper, for the objective function of the proposed VPPs aggregation strategy model, appropriate weight values for structural indicator λ_{str} and functional indicator λ_{fun} are selected. Various test weight values λ are examined to derive corresponding VPPs division objective functions. The Louvain Algorithm is then employed for clustering. Through comparison and analysis of the performance of structural and functional indicators under different cluster division weight values, weight values that yield optimal performance for both indicators are chosen. These selected weight values form the basis of the optimal cluster division scheme for the power distribution network. The results of the cluster division of the virtual power plant under different weight values are illustrated in Fig. 7.

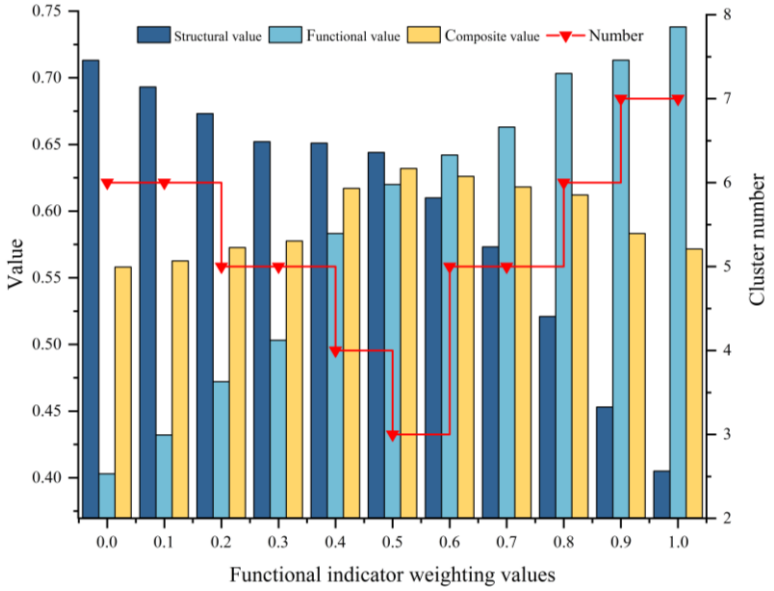

Fig. 7 VPPs division data with different weight values

Upon analyzing Fig. 7, it becomes evident that as the weight value of the functional indicator increases, the value of the structural indicator of VPPs decreases, while the value of the functional indicator increases. Consequently, the comprehensive performance indicators of the clusters initially increase and then decrease, and the number of VPP follows a pattern of decreasing and then increasing. The comprehensive indicators of VPPs are maximized when the number of clusters is minimized, aligning with the division principle of strong coupling within the cluster, independence between clusters, and no isolated nodes within the cluster.

At a weight value of 0.5 for the functional indicator, the comprehensive indicator of VPPs is maximized, and the number of VPPs is minimized, consistent with the aforementioned division principle. Consequently, the optimal weights are determined as $\lambda_{\text{str}} = 0.5$ and $\lambda_{fun} = 0.5$.

Taking the above optimal weight value, the cluster structural indicator $\varphi_{\text{str}} = 0.644$, functional indicator $\varphi_{fun} = 0.6200$. At this time, the cluster not only has good structural characteristics, but also has good flexibility of the functional characteristics. The specific cluster division results are shown in Fig. 8.

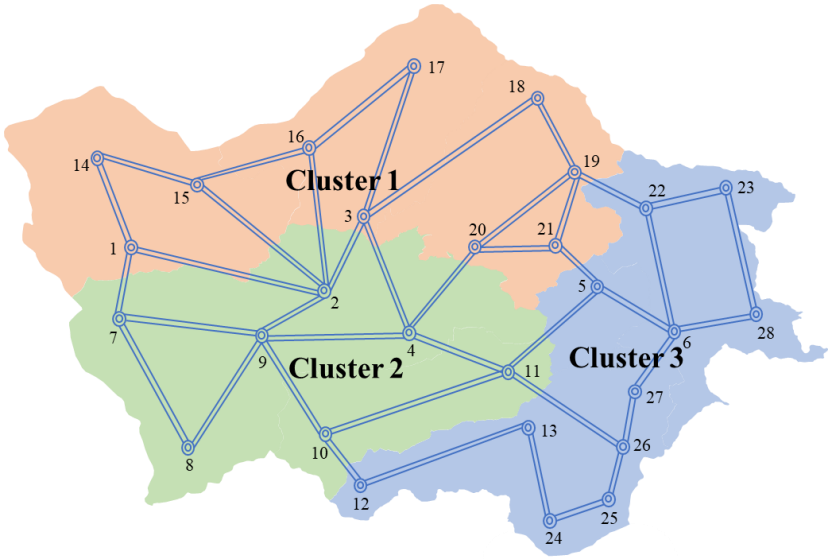

Fig. 8 Graph of VPPs division results

To validate the effectiveness of the division method proposed in this paper, considering functional metrics, a case comparison method is employed. This paper analyzes the indicator results, focusing on the active power balance time and the cluster flexibility deficit. case 1 solely relies on division based on the electrical distance

modularity indicator, whereas case 2 incorporates the indicator proposed in this paper for division. Fig. 9 illustrates the results of case 1 cluster division.

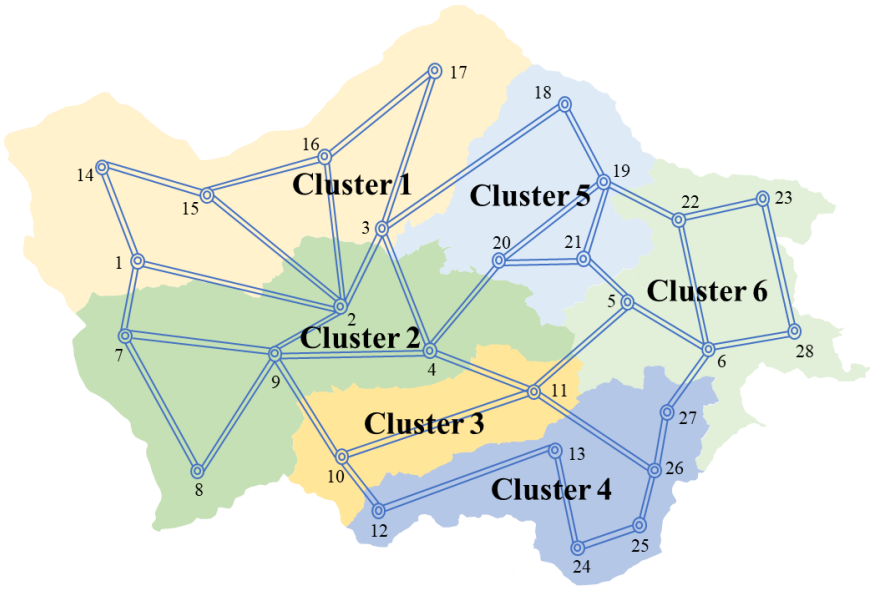

Fig. 9 Case 1 clustering results

Fig. 9 illustrates that when solely relying on structural indicator as the sole optimization objective for flexibility resource aggregation, the division yields six clusters. At this point, the structural indicator is maximized, and the nodes within the clusters are closely connected. However, due to the lack of consideration for the regulation ability of the nodes within the clusters, the functional indicator is minimized. A comparison of the cluster division results is provided in Table 2.

Table 2 A comparison of the cluster division results

Case	φ_{str}	φ_{fun}	Number of clusters	Active power balance ratio	Upward flexibility total shortfall	Downward flexibility total shortfall
Case 1	0.7131	0.4030	6	12.33%	52.43MW	103.67MW
Case 2	0.6440	0.6200	3	35.85%	22.82MW	24.39MW
comparative	-0.0691	0.2170	-3	23.52%	56.49%	76.47%

Table 2 demonstrates that Case 2 exhibits a reduction of 0.0691 in structural indicator compared to Case 1, while still maintaining structural indicator above 0.6. This ensures that the clusters maintain strong structural characteristics. Additionally, Case 2 shows a 53.85% increase in functional indicator, indicating enhanced flexibility characteristics within the clusters. Specifically, Case 2 increases the active power balance ratio by 23.52%, reduces cumulative upward flexibility deficits by 56.49%, and decreases cumulative downward flexibility deficits by 76.47%. This improvement is attributed to the consideration of matching flexibility resource supply capacity and demand within Case 2. By allocating larger supply capacity flexibility resources to clusters with greater demand. This approach leverages the flexibility resource regulation capacity of both sources and loads, thereby enhancing the autonomous performance characteristics of the clusters.

Therefore, the division method proposed in this paper not only ensures close linkage of nodes within clusters and loose inter-cluster connections but also maximizes the functional characteristics of the clusters.

6.2.2 Optimization results for two-stage scheduling of VPP clusters

To showcase the effectiveness of the VPPs in addressing the uncertainty of wind and solar output in real-time scenarios， this section selects the optimal VPP clusters division case in Section 6.1.1 as an analysis. The simulation entails conducting a two-stage scheduling optimization of VPPs, with scheduling measurements carried out over a 24-hour optimization period and a time step of 1 hour. Based on the typical daily scenario data of each node in Fig. 5 and the VPPs division result diagram in Fig. 8. The typical daily forecast output

and load demand of Non-AGU within each VPP in the day-stage are obtained as shown in Fig. 10 and Fig. 11.

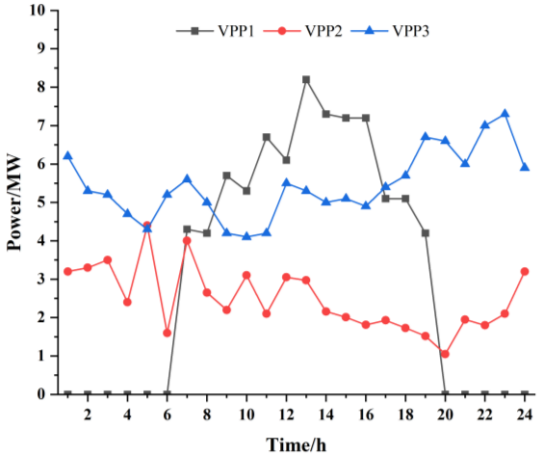

Fig. 10 Non-AGU day-ahead forecast output

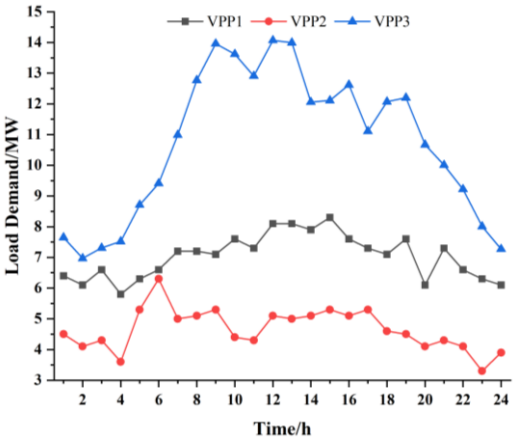

Fig.11 Load forecast demand

In this paper, the VPP balance power is selected as the uncertainty variable, and the balance power deviation value obeys normal distribution. The confidence interval is used to find the fluctuation range of the balance power of each VPP as shown in Fig. 12.

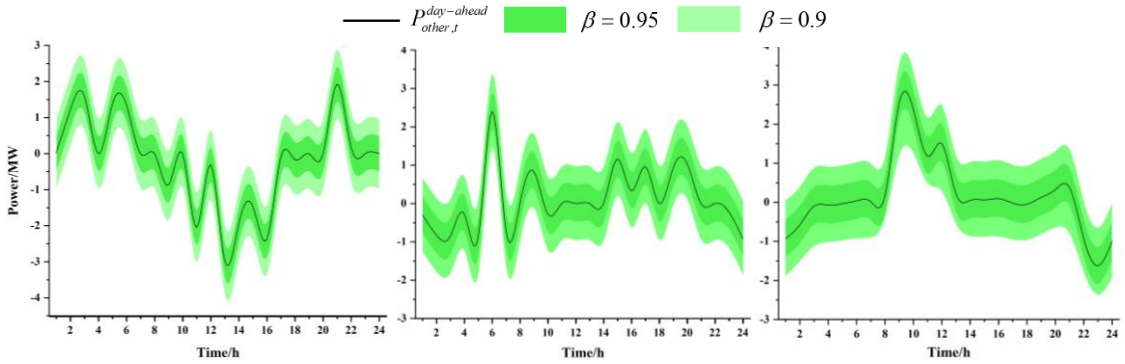

(a) VPP1 (b) VPP2 (c) VPP3

Fig. 12 Range of fluctuations in balancing power requirements

Fig. 12 illustrates the range of fluctuations in balancing power requirements. Decision-makers can adjust β flexibly to ensure optimal robustness and system synthesis goals, especially when facing varying proportions of renewable energy sources. In this paper, a confidence level of $\beta = 0.95$ is chosen to evaluate the effectiveness of the two-stage scheduling optimization for VPPs.

Moreover, a robust coefficient of $\Gamma = 0.5$ is selected for the two-stage scheduling optimization of VPPs. This optimization aims to minimize the average energy generation cost of the clusters. Fig. 13 displays the resulting day-ahead optimal scheduling strategies of VPP_1, VPP_2, VPP_3.

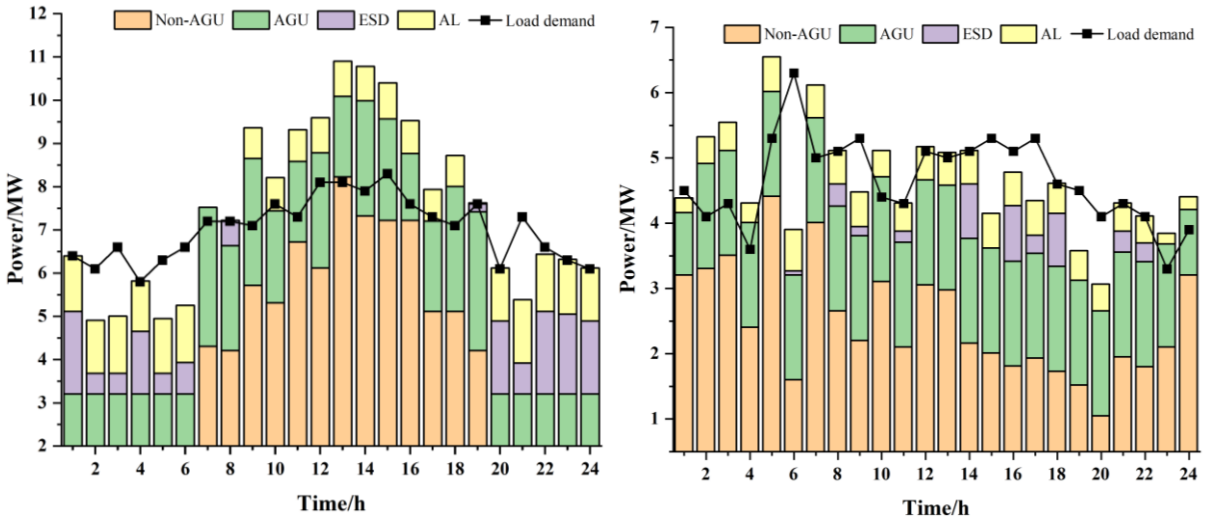

(a) VPP_1 (b) VPP_2

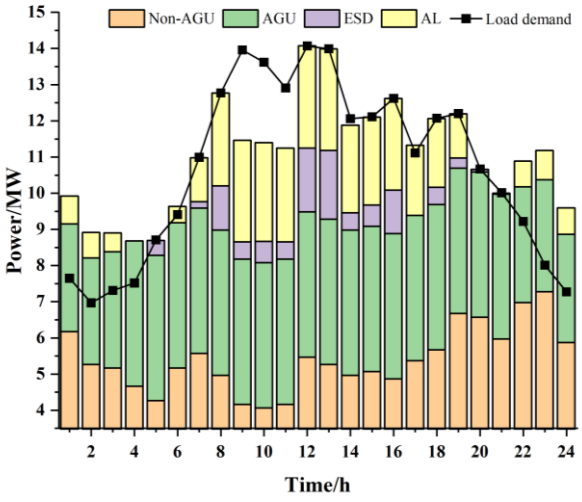

(c) VPP_3

Fig. 13 Graph of unit output and load profile

Fig. 13(a) shows that VPP_1 achieves internal source-load balance at 1:00, 4:00, 8:00, 20:00, and 23:00-24:00 hours, with its internal source output exceeding load demand in most instances during Non-AGU output hours (07:00-19:00). This phenomenon can be attributed to the substantial output of PV during daylight hours, which challenges the internal regulated resources of VPP_1 to manage large PV output. Consequently, VPP_1 needs to dispatch power internally to achieve internal supply-demand balance. In Fig. 13(b) and (c), it's observed that VPP_2 achieves source-load balance primarily at 8:00, 11:00-14:00, and 21:00-22:00, while VPP_3 achieves source-load balance for most of the time at 6:00, 8:00-9:00, and 12:00-21:00. This indicates that the structural-functional aggregation optimization strategy for VPPs better aligns with source-load balance, reducing instances of surplus power and minimizing wind and solar power losses. Consequently, it enhances the internal balance of the VPPs.

Table 3 Operating costs for each unit in the day-ahead stage

	Cost of Non-AGU/¥	Cost of AGU/¥	Cost of ESD/¥	Cost of AL/¥	Cost of Other/¥	Total
VPP_1	9192	10073	9798	10147	15905	55115
VPP_2	7167.6	4640.5	5801.25	4761.5	10336	32706.85
VPP_3	15648	14214	9216	15584	8820	63482

Table 3 presents the operating costs of each VPP under the optimal scheduling strategy from the day-ahead stage. Notably, VPP_3 exhibits the highest running cost, due to its significant consumption of Non-AGU output. Conversely, VPP_1 incurs the highest cost for required balancing power, mainly because the output of

Non-AGU within VPP_1 exhibits time-specific characteristics. During periods of high PV output, the internal adjustable resources struggle to absorb the surplus PV output, necessitating external interaction to maintain balance. In the real-time stage, VPPs adjust unit output to mitigate the uncertainty of balancing power. Table 4 presents the data of the optimal scheduling strategy of VPPs in both the day-ahead and real-time stages

Table 4 The results of the optimization of each VPP

		VPP_1	VPP_2	VPP_3
Operating cost (¥)		55115	32706.85	63482
Adjustment cost (¥)		1554.87	1429.43	1077.94
Cost		56669.87	34136.28	64559.94
Day-ahead Power/MW	Non-AGU	76.6	59.73	130.4
	AGU	66.92	37.12	90.34
	ESD	20.72	6.89	20.28
	AL	21.70	10.50	34.55
	Other	19.88	12.92	11.03
	Load demand	168.6	111.9	257.23
Real-time Power/MW	Non-AGU	86.43	68.72	138.92
	AGU	64.23	40.54	88.37
	ESD	24.51	10.08	21.36
	AL	22.02	10.64	36.27
	Other	31.40	20.41	19.47
	Load demand	187.03	127.49	290.09
Adjustment/MW	Non-AGU	9.83	8.99	8.52
	AGU	-2.68	3.58	-1.97
	ESD	3.79	3.20	1.08
	AL	0.32	0.13	1.73
	Other	11.52	7.49	8.44
	Load demand	18.43	15.59	3.86

Table 4 illustrates an increase in the required balancing power during the real-time stage, amounting to 11.52MW, 7.49MW, and 8.44MW. Correcting the day-ahead output helps reduce fluctuations in AGU, ESD, and AL. Notably, ESD exhibits the largest deviation in corrected output compared to AGU and AL. This discrepancy arises because the day-ahead dispatch strategy struggles to achieve the 'full' and 'empty' conditions of ESD, resulting in a wider adjustable space for ESD. The scheduling strategy's inability to fully address the 'full' and 'empty' conditions of ESD amplifies the adjustable space, especially when deviations occur during the real-time stage. Based on the above analysis, it's evident that the two-stage scheduling optimization model of VPP clusters enables self-scheduling within each VPP during the real-time stage.

To delve further into the mechanism of internal unit adjustment within VPPs when deviations in required balancing power occur during the real-time stage, this paper selects ESD with the largest corrected output deviation in VPP_1. A comparative analysis of the day-ahead and real-time stages of the output situation and its SOC is conducted, with results presented in Fig. 14.

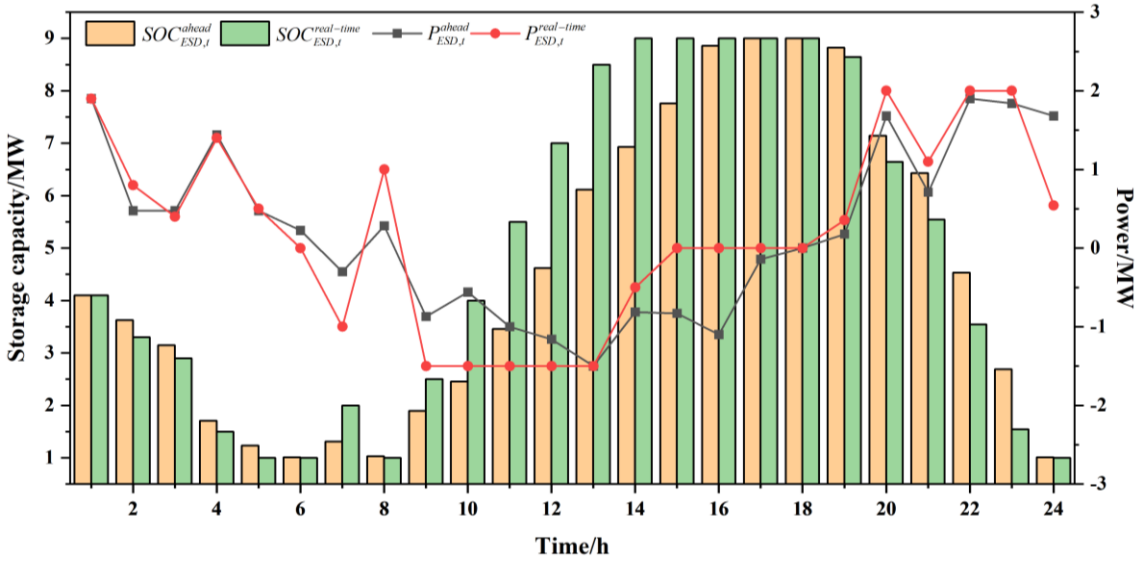

Fig. 14 Comparison of ESD day-ahead and real-time stages output and capacity percentage in VPP_1

Fig. 14 illustrates the scheduling results of ESD in both the day-ahead and real-time stages. It's evident that the charging and discharging rate of ESD during the real-time stage significantly exceeds that of the day-ahead stage. Specifically, during periods when PV is not generating power (00:00-06:00 & 20:00-24:00), ESD is in a charging state. Notably, in the real-time stage, ESD reaches the full release state at 05:00, whereas in the day-ahead scheduling plan, this state is achieved only at 06:00. Additionally, SOC of ESD from 20:00 to 24:00 exhibits a faster decreasing trend in the real-time stage compared to the day-ahead stage. During periods of PV output (07:00 & 19:00), ESD achieves full storage state at 15:00 in the real-time stage and at 17:00 in the day-ahead stage. Consequently, in the event of a deviation in the required balancing power of VPP_1 during the real-time stage, the charging and discharging rate of ESD is further increased to mitigate the large-scale deviation in the required balancing power of VPP_1.

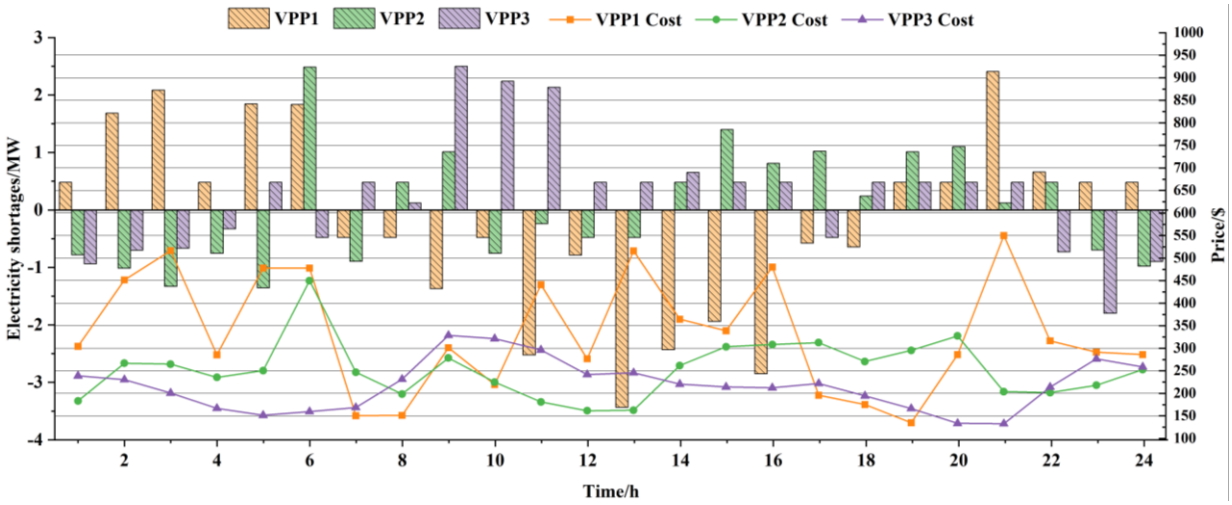

Fig. 15 Data reported to the control center by each VPP after the day-ahead and real-time dispatch strategy

Fig. 15 depicts the required balancing power and running cost data for each VPP following day-ahead and real-time scheduling. Taking VPP_1 as an example, it's evident from Fig. 15 that during PV non-power hours (00:00-06:00 & 20:00-24:00), VPP_1 requires positive balancing power. This indicates that VPP_1 needs to purchase power from the grid to maintain its power balance. Due to the higher purchasing cost during these hours, the average cost of energy generation for VPP_1 is larger than that of VPP_2 and VPP_3. Similarly, during periods of significant PV output (09:00-16:00), VPP_1 still needs to purchase power from the grid to maintain its power balance, resulting in a higher average cost of energy generation enter compared to VPP_2 and VPP_3. Moreover, during the peak PV output hours (09:00-16:00), VPP_1 requires negative balancing power, leading

to a substantial amount of wind and solar energy curtailment and an increase in penalty costs. Consequently, the average cost of energy generation for VPP_1 remains higher during this period.

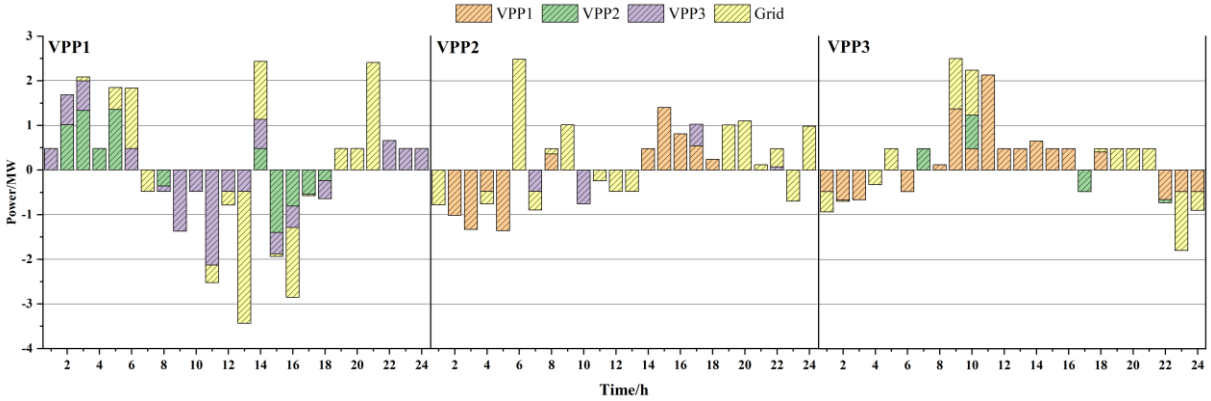

Fig. 16 Dynamic balancing strategy for the real-time stage of VPPs

Fig. 16 presents the outcomes of the dynamic balancing strategy implemented during the real-time stage of VPPs. To illustrate, this paper take the VPP_1 2:00 time slot as an example. During this period, the internal required balancing power for the clusters is calculated to be 1.685 MW, indicating the need for power supply from other VPPs or the grid. Meanwhile, VPP_2 and VPP_3 generate surplus energy of 1.0133 MW and 0.7 MW. Notably, the average cost of generation power from VPP_2 is higher than that of VPP_3. To minimize the average cost of generation power to the system, the remaining power generated by VPP_2 is preferentially allocated to VPP_1, and VPP_3 fills the remaining 0.6717 MW gap in VPP_1's power supply. Finally, the remaining 0.0283 MW of power within VPP_3 is directed to the power grid. This analysis demonstrates that the dynamic balancing strategy of VPPs effectively utilizes new energy resources on a larger scale, mitigates the issue of significant deviations in required balancing power that are challenging to rectify within a short timeframe.

Table 7 Comparison before and after dynamic balancing of VPPs

	Upward Flexibility Shortfall/MW	Downward adjustment of flexibility shortfall/MW	Required balancing power/MW	Total cost/¥	Average cost of energy generation ($/MW)
pre-balance	34.00	37.27	71.27	155366.09	273.89
after-balance	15.69	13.99	29.67	122085.29	215.21
difference	18.32	23.29	41.60	33280.80	58.68

Table 7 presents a comparison of dynamic balancing data for VPPs. From the table, it's evident that following dynamic balancing, there are notable improvements: VPPs upward flexibility shortage decreases by 53.87%; the downward flexibility shortage decreases by 62.47%; the required balancing power decreases by 58.37%; the total cost of VPPs decreases by 21.42%; and the average cost of generation energy decreases by 58.68¥/MW. This analysis demonstrates that the dynamic balancing strategy effectively mitigates the problem of insufficient flexibility adjustment capacity within VPPs, thereby ensuring the safe and stable operation of the distribution network. Furthermore, the strategy contributes to a reduction in the average cost of energy generation, thus promoting the economic operation of the distribution network.

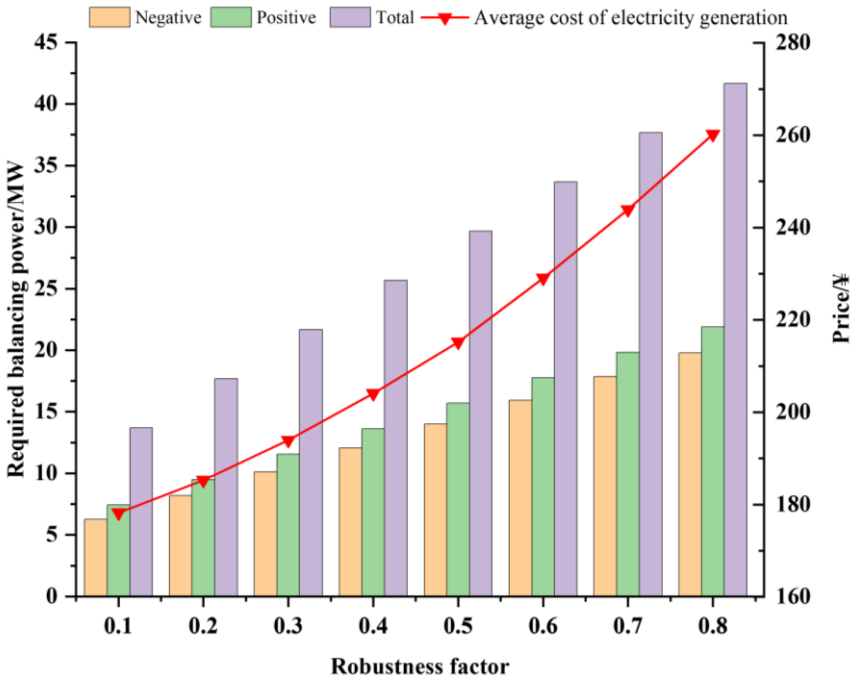

Fig. 17 Results of VPPs with different robustness coefficients

Fig. 17 illustrates the variation in deviation power and average energy generation cost of VPPs with different robustness coefficients. The figure demonstrates that as the robustness coefficient increases, the positive deviation, negative deviation, and total deviation of VPPs exhibit a increase, while the average energy generation cost of VPPs demonstrates a non-linear increase. Analyze the reason is mainly when the wind and other new energy power fluctuations on a large scale, VPPs is difficult to adjust the space through its own flexibility to suppress the new energy power fluctuations, resulting in a large number of wind and light abandonment, resulting in the deviation cost and the cost of adjustment of the exponential growth.For individuals not averse to risk, setting the robustness coefficient at 0.5 strikes a balance between the economic and safety considerations of VPPs, achieving optimal overall scheduling optimization strategy.

6.2.3 Results of the distribution of benefits from VPPs

Each unit is aggregated to form a VPP, enabling it to participate in the overall scheduling of the distribution network independently while also reaping benefits as part of VPPs. To achieve this, it is imperative to devise a comprehensive benefit allocation plan for each VPP. The benefit allocation strategy is delineated into two distinct components. Consequently, this paper conducts a two-layer benefit allocation process for the optimal scheduling strategy of VPPs obtained in Section 6.2.2.

Table 8 Profitability of possible combinations of external clusters of VPPs

	Avaliable VPP			Profit/¥
	VPP_1	VPP_2	VPP_3	
1	✓			92139.23
2		✓		73622.28
3			✓	138214.68
4	✓	✓		184467.59
5	✓		✓	250700.79
6		✓	✓	219188.93
7	✓	✓	✓	337370.26

Table 8 evaluates the influence of various VPPs participating in cooperation on the outcomes of benefit allocation. It provides the profits of potential combinations of external clusters of VPPs and computes the benefit factor of each VPP based on Eq. (42)-(43). Subsequently, the Shapley value method is employed to

equitably distribute the incremental benefits arising from the cooperation of VPPs. The distribution results are presented in Table 9.

Table 9 Results of the distribution of benefits of external clusters of VPPs

	Benefit factor	Shapley value distribution profit/¥	Incremental gain/¥
VPP1	0.4549	107328.76	15189.53
VPP2	0.2603	82314.35	8692.07
VPP3	0.2849	147727.15	9512.47

Table 9 demonstrates the benefit factors and the allocated incremental benefits of the external clusters of VPPs, the benefit factors calculated by VPP_1, VPP_2, and VPP_3 are 0.4549, 0.2603, and 0.2849. The incremental benefits of 33280.8¥ generated by VPP co-operation are allocated according to the benefit factors, and the profits gained by VPP_1 , VPP_2 , and VPP_3 are 45.49% and 26.03% and 28.49% of the total incremental benefits. The main reason is that VPP_1 contains a large number of PV and has a large adjustable depth. When PV is enough in power, VPP_1 can provide the internal flexibility to consume the excess power generated in the remaining VPPs. After the external benefit allocation of VPP clusters, this paper use VPP_1 as an example to further analyse the effectiveness of the internal unit benefit allocation strategy.

Table 10 Running risk and costs of possible combinations of VPP_1 internal units

	DERs				factor	
	Non-AGU	AGU	ESD	AL	Risk	Cost
1	✓				7.66	63895
2		✓			4.85	66571
3			✓		6.12	68568
4				✓	6.70	67595
5	✓	✓			4.14	60696
6	✓		✓		5.47	61496
7	✓			✓	5.97	61148
8		✓	✓		4.95	61868
9		✓		✓	5.14	63585
10			✓	✓	5.86	64771
11	✓	✓	✓		3.75	59067
12	✓	✓		✓	4.33	59885
13	✓		✓	✓	4.85	58917
14		✓	✓	✓	3.30	59868
15	✓	✓	✓	✓	3.14	56669

Table 10 considers the deviation power and running costs of different types of units after participating in the aggregation to form VPP. It calculates the risk factor and cost factor of different types of units according to Eqs. (44)-(45). Subsequently, the Shapley value method is utilized to equitably allocate the incremental benefits generated from the participation in centralized dispatch of VPP formed by the aggregation of each unit. Furthermore, the weights of the risk factor and the cost factor are set to both be 0.5. The results of unit benefit allocation within VPP_1 are presented in Table 11.

Table 11 Results of the incremental benefit allocation for the internal module of VPP_1

	cost factor	risk factor	Incremental cost benefit (¥/MWh)	Incremental return on risk (¥/MWh)	Total share of proceeds (¥/MWh)	Shapley value (¥/MWh)
Non-AGU	0.44	0.10	78.01	17.87	47.94	77.03
AGU	0.25	0.47	43.36	83.62	63.49	57.24
ESD	0.19	0.27	33.41	46.61	40.00	21.84
AL	0.12	0.16	20.97	27.63	24.30	19.63

Table 11 shows the results of the incremental benefit allocation of internal units in the VPP_1. Compared with the traditional Shapley method, Non-AGU needs to make a profit of 29.09¥/MWh due to the uncertainty of output, and AGU, ESD, and AL gain 6.24¥/MWh, 18.16¥/MWh, and 4.67¥/MWh. This increase in profit

allocation for AGU, ESD, and AL units is attributed to their ability to provide flexible space, thereby mitigating system operation risks. Fig. 18 shows the percentage of benefits allocated to each unit for different scenarios of VPP_1 , VPP_2 and VPP_3 .

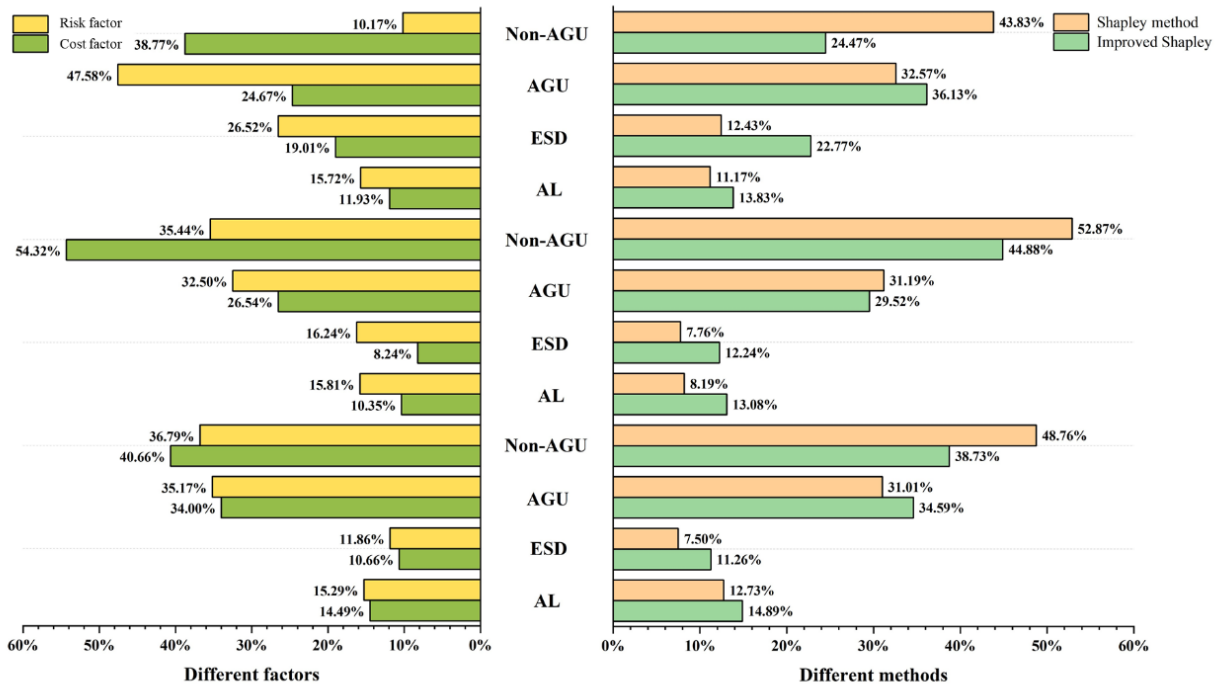

Fig. 18 Percentage distribution of the benefits of each unit under different methods and different factors

Fig. 18 illustrates that when the risk factor is utilized as the distribution dimension, there is a notable decrease in the proportion of benefits allocated to Non-AGU, accompanied by a significant increase in the proportion allocated to AGU, ESD, and AL. Conversely, if the cost factor is employed as the distribution metric, the benefits received by Non-AGU experience a substantial increase while those received by the other units decrease significantly. Furthermore, from the perspective of overall benefit allocation, the incorporation of risk and cost factors leads to a reduction in the incremental benefits of Non-AGU and an increase in those of AGU, ESD, and AL. This adjustment aligns is more in line with the actual contribution of AGU, ESD, and AL in the power system. Thus, it validates the effectiveness of the internal unit benefit allocation strategy proposed in this paper.

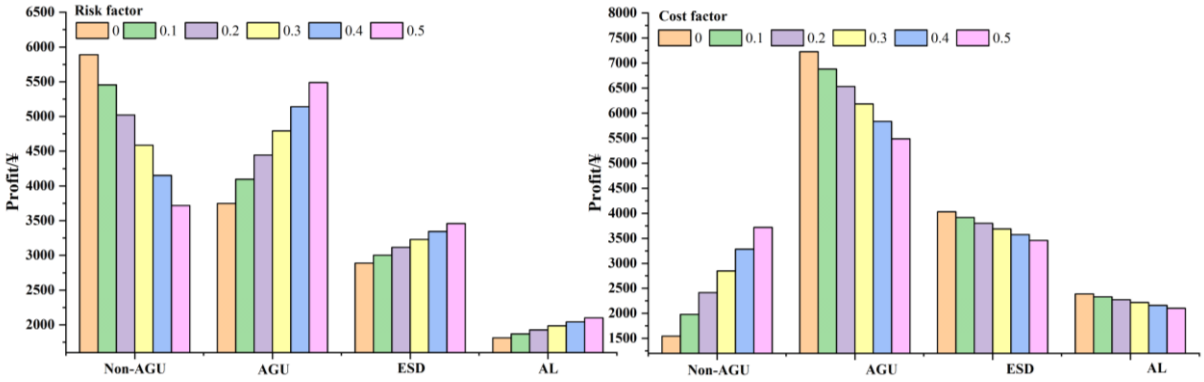

Fig. 19 Results of sensitivity analyses under different weights of influence factors for VPP_1

Fig. 19 presents the sensitivity analysis results of VPP_1 with varying weights of impact factors. As depicted in the figure, an increase in risk factors leads to a gradual decrease in the benefits of Non-AGU, while the benefits of AGU, ESD, and AL show an increasing trend. This trend is attributed to the uncertainty associated with Non-AGU output, which exacerbates the risk of power system operation. AGU, ESD, and AL

units incur operating costs and deviation adjustment costs resulting in increased costs when they receive real-time adjustments, so their cost factors are small. Consequently, their cost factors remain relatively small. In conclusion, the synergistic benefit allocation strategy devised for VPP clusters effectively addresses both the external clusters of VPPs and the multidimensional impacts of risk and cost on internal units. This approach ensures the attainment of an optimal benefit balancing strategy for each entity.

7 Conclusion

This paper delves into the distribution network topology and the flexibility requirements of VPPs, establishes an optimization strategy for structural-functional aggregation in VPPs. It devises a two-stage scheduling optimization model aimed at minimizing the average energy generation cost. At the same time, this paper introduces the risk factor and the cost factor, and proposes a balanced allocation strategy of synergistic benefits of VPPs. The analysis is exemplified through calculations conducted in Huangyuan County, Xining City, Qinghai Province. The conclusions drawn are as follows:

(1) The proposed structure-function aggregation optimization strategy for VPPs is conducive to maximizing the use of distributed energy flexibility capacity and generating structurally stable VPPs with sufficient flexibility. The proposed strategy enhances the active power balance rate of VPPs by 23.52%. It reduces the aggregate upward flexibility deficit by 56.49% and the downward flexibility deficit by 76.47%.

(2) The proposed two-stage scheduling optimization model for VPPs shows good economic benefits. The two-stage robust optimization used is able to effectively portray the uncertainty of the real-time output of Non-AGU. The proposed model reduces the required balancing power by 58.37%. At the same time, it decreases the total cost of VPPs by 21.42%, and lowers the average cost of supplying energy to 58.68¥/MW.

(3) The proposed synergistic benefit allocation strategy of VPPs reflects the characteristics of different types of units and ensures the fairness of benefit allocation. Utilizing the proposed synergistic benefit allocation strategy, In VPPs, VPP_1, VPP_2, VPP_3 obtained by VPPs for 45.49%, 26.03%, and 28.49% of the total incremental gains. Then, Non-AGU needs to make a profit of 29.09¥/MWh due to the uncertainty of output in VPP_1. AGU, ESD and AL gain 6.24¥/MWh, 18.16¥/MWh, and 4.67¥/MWh.

(4) With the ongoing advancement of intelligent power systems, evolving distribution network topologies increasingly replace traditional transmission structures. Future research endeavors will explore the impact of corresponding network structure changes on cluster division, particularly concerning the opening and closing states of contact lines between nodes. Additionally, there will be a focus on uncertainty portrayal and optimal configuration of Non-AGU units for cooperative operation methods of VPPs.

Appendix

According to Eq. (40), the C&CG algorithm is used to solve the three-layer robust optimization problem through subproblem iterations. The main problem consists of the first stage model and sub-problems to find the new energy unit output constraints for the worst case new energy scenario, and the main problem during the *ith* iteration is as follows:

$$\min_{\boldsymbol{x}_1 \in \boldsymbol{\Omega}_1} \left(\boldsymbol{c}_1\right)^T \boldsymbol{x}_1 + \boldsymbol{\eta}$$
$$s.t. \begin{cases} \boldsymbol{x}_1 \le \boldsymbol{a} \\ \boldsymbol{\eta} \ge \boldsymbol{b}^T \boldsymbol{P}_{\text{other},k}^{2*} + \left(\boldsymbol{c}_2\right)^T \boldsymbol{x}_{2,k} \\ \boldsymbol{D}\boldsymbol{x}_{2,k} \le \boldsymbol{E}\boldsymbol{x}_1 + \boldsymbol{P}_{\text{other},k}^{1} + \boldsymbol{d} \\ 0 \le k \le i\text{-}1 \end{cases} \tag{1}$$

Where: $\boldsymbol{P}_{\text{other},k}^{2*}$ is the equilibrium power required for the worst case scenario VPP solved by the lower level problem; $\boldsymbol{x}_{2,k}$ is the new optimization variable added to the main problem; $\boldsymbol{\eta}$ is the value of the objective

function for the second stage to be optimized.

The subproblem is a two-layer max-min optimization problem, which can be transformed into a maximisation problem by means of strong dyadic theory by transforming the inner minimization problem into a maximization problem, and the *ith* iteration subproblem model after the transformation is:

$$\max\left(\boldsymbol{b}^T \boldsymbol{P}_{\text{other}}^2 + \left(\boldsymbol{E}\boldsymbol{x}_{1,i} + \boldsymbol{F}\boldsymbol{P}_{\text{other}}^1 + \boldsymbol{d}\right)^T \boldsymbol{\varphi}\right)$$
$$s.t.\begin{cases} \boldsymbol{D}\boldsymbol{\varphi} \le \boldsymbol{c}_2 \\ \boldsymbol{\varphi} \le 0 \end{cases} \tag{2}$$

Where: $\boldsymbol{\varphi}$ is the dyadic variable of the second stage constraints. It should be noted that the new energy available output is introduced in the second stage model to guarantee the feasibility of the subproblem.

Acknowledgments

This work was partially supported by the National Natural Science Foundation of China (Grant Nos. 72274060, 71904049, 72174062, 72074074), the Beijing Social Science Fund (23JCB039), and the Beijing Natural Science Foundation (9242014).

References

[1] Jin H, Sui J. Transformative energy utilisation technologies-distributed energy systems[J]. Distributed Energy, 2016, 1(01): 1-5.

[2] Ju L, Lv S, Li. A review on the research of new power system demand-side flexibility resource spatio-temporal co-optimization and dynamic equilibrium mechanism[J/OL]. Electric Power Construction,1-27[2024-02-27].

[3] Loßner M, Böttger D, Bruckner T. Economic assessment of virtual power plants in the German energy market â□" A scenario-based and model-supported analysis[J]. Energy Economics, 2017, 62125-138.

[4] Yakubu A, Alex K, Euan P. Unlocking the economic viability of marginal UKCS discoveries: Optimising cluster developments[J]. Energy Economics, 2021, 97

[5] Ruan H, Gao H, Gooi H, et al. Active distribution network operation management integrated with P2P trading[J]. Applied Energy, 2022, 323

[6] Fu X, Zhu L, Zhao Z et al. Calculation of max power supply capacity of zonal flexible interconnected grids taking into account dynamic voltage stability constraints[J]. Grid Technology,2023,47(02):553-563.

[7] Zheng F, Meng X, Xu T, et al. Voltage Zoning Regulation Method of Distribution Network with High Proportion of Photovoltaic Considering Energy Storage Configuration[J].Sustainability,2023,15(13).

[8] Marcos T, M. H, Ahmad J R, et al. An Interval-based privacy - Aware optimization framework for electricity price setting in isolated microgrid clusters[J].Applied Energy,2023,340

[9] Ruth D, Sebastiano V, Miguel C, et al. Analysing decarbonizing strategies in the European power system applying stochastic dominance constraints[J]. Energy Economics, 2021, 101

[10] Hu D, Ding M, Bi R et al. Analysis of the impact of photovoltaic and wind power complementarity on the planning of high penetration renewable energy cluster access[J]. Chinese Journal of Electrical Engineering,2020,40(03):821-836.

[11] Zhang Y, Yue M, Wang J, et al. Multi-Agent Graph-Attention Deep Reinforcement Learning for Post-Contingency Grid Emergency Voltage Control.[J].IEEE Transactions on Neural Networks and Learning Systems,2024,PP

[12] Fan W, Tan Q, Zhang A, et al. A Bi-level optimization model of integrated energy system considering wind power uncertainty[J]. Renewable Energy, 2023, 202973-991.

[13] Arocena P, Plana G, Peña S. A model for the competitive benchmarking of energy costs[J]. Energy Economics, 2024, 131107385-.

[14] Ju L, Yin Z, Zhou Q, et al. Nearly-zero carbon optimal operation model and benefit allocation strategy for a novel virtual power plant using carbon capture, power-to-gas, and waste incineration power in rural areas[J]. Applied Energy, 2022, 310: 118618.

[15] Wang D, Liu Y, Wang Y, et al. Allocation of coal de-capacity quota among provinces in China: A bi-level multi-objective combinatorial optimization approach[J]. Energy Economics, 2019, 87

[16] Ramea K, Bunch S, Yang C, et al. Integration of behavioral effects from vehicle choice models into long-term energy systems optimization models[J]. Energy Economics, 2018, 74663-676.

[17] Jihyeok J ,Chan-Oi S ,Deok-Joo L, et al. Optimal energy procurement with long-term photovoltaic energy contracts considering generation uncertainty. A two-dimensional auction approach[J]. Applied Energy, 2024, 356122383-.

[18] Ding B, Marek M, Zbigniew N, et al. Optimizing the technology pathway of China's liquid fuel production considering uncertain oil prices: A robust programming model[J]. Energy Economics, 2022, 115

[19] MA C, Dong C, LV Z, et al. Short-term trading and optimal operation strategy for commercial virtual power plant considering uncertainties[J]. Power System Technology, 2016,40(5): 1543-1549

[20] Sun Y, Liu X, Wang R, et al. Distributed Optimal Scheduling of VPP based on EST: An ADMM algorithm based on historical data online transfer[J]. Applied Energy, 2023, 347: 121416.

[21] Barrionuevo R, Pio C, Martins E, et al. Two-stage stochastic energy procurement model for a large consumer in hydrothermal systems[J]. Energy Economics, 2022, 107:105841-.

[22] Zhang Y, Zhao H, Li B. Distributionally robust comprehensive declaration strategy of virtual power plant participating in the power market considering flexible ramping product and uncertainties[J]. Applied Energy, 2023, 343: 121133.

[23] Ranjan P, Kumar S, Prajwal E, et al. An explainable artificial intelligence approach to understanding drivers of economic energy consumption and sustainability[J]. Energy Economics, 2023, 125

[24] Pu Y, Li S, Zhang C, et al. High expression of CXCR3 is an independent prognostic factor in glioblastoma patients that promotes an invasive phenotype[J]. Journal of neuro-oncology, 2015, 122(1): 43-51.

[25] Zhou D, Wu C, Sui Q, et al. A novel all-electric-ship-integrated energy cooperation coalition for multi-island microgrids[J]. Applied Energy, 2022, 320

[26] Zhao L, Xue Y, Sun H, et al. Benefit allocation for combined heat and power dispatch considering mutual trust[J]. Applied Energy, 2023, 345

[27] Diva A M ,Rémy R ,Vincent D , et al. A two-stage management strategy for the optimal operation and billing in an energy community with collective self consumption[J]. Applied Energy, 2022, 310

[28] Chen Y, Park B, Kou X, et al. A comparison study on trading behaviour and profit distribution in local energy transaction games[J]. Applied Energy, 2020, 280115941-.

[29] Ju L, Lu X, Yang S, et al. A multi-time scale dispatching optimal model for rural biomass waste energy conversion system-based micro-energy grid considering multi-energy demand response[J]. Applied Energy, 2022, 327

[30] Yang S, Tan Z, Zhao R, et al. Operation optimization and income distribution model of park integrated energy system with power-to-gas technology and energy storage[J]. Journal of Cleaner Production, 2020, 247: 119090.

[31] Pan H, Fang J. Research on benefit allocation of comprehensive energy services unDRE the background of green development concept[J]. Fresenius Environmental Bulletin, 2021, 30(6): 6188-6197.

[32] Diego G, Esteban G, Guillermo G. Ramping ancillary service for cost-based electricity markets with high penetration of variable renewable energy[J]. Energy Economics, 2020, 85

[33] Subramanyam A S, Zhang X. Effect of Loss of Load Probability Distribution on Operating Reserve Demand Curve Performance in Energy-Only Electricity Market[J]. IEEE Transactions on Power Systems, 2020, 35(4): 3297-3300.

[34] Wang J, Xie N, Huang C, et al. Two-stage stochastic-robust model for the self-scheduling problem of an aggregator participating in energy and reserve markets[J]. Protection and Control of Modern Power Systems, 2023, 8(1).